

Targeting the mosquito prefoldin–chaperonin complex blocks *Plasmodium* transmission

Received: 22 November 2024

Accepted: 27 January 2025

Published online: 6 March 2025

 Check for updates

Yuemei Dong¹, Seokyoung Kang¹, Simone L. Sandiford  ¹, Andrew Pike¹, Maria L. Simões  ^{1,3}, Ratawan Ubalee², Kevin Kobylinski² & George Dimopoulos  ¹✉

The *Plasmodium* infection cycle in mosquitoes relies on numerous host factors in the vector midgut, which can be targeted with therapeutics. The mosquito prefoldin complex is needed to fold proteins and macromolecular complexes properly. Here we show that the conserved *Anopheles* mosquito prefoldin (PFDN)–chaperonin system is a potent transmission-blocking target for multiple *Plasmodium* species. Silencing any prefoldin subunit or its CCT/TRiC partner via RNA interference reduces *Plasmodium falciparum* oocyst loads in the mosquito midgut, as does co-feeding mosquitoes with PFDN6-specific antibody and gametocytes. Inhibition of the PFDN–CCT/TRiC chaperonin complex results in the loss of epithelial and extracellular matrix integrity, which triggers microorganism-mediated anti-*Plasmodium* immune priming and compromises the parasite’s laminin-based immune evasion. Mouse malaria transmission-blocking vaccine and antibody co-feeding assays support its potential as a multispecies transmission-blocking target for *P. falciparum* and *Plasmodium vivax*. Further study is needed to determine the potential of this system as a transmission-blocking vaccine target.

Malaria, caused by the protozoan parasite *Plasmodium*, which is transmitted by *Anopheles* mosquitoes, is one of the deadliest diseases because of the lack of highly effective malaria vaccines as well as the parasites’ and mosquitoes’ emerging resistance to drugs and insecticides, respectively. During its complex journey through the mosquito gut, haemolymph and salivary glands, the parasite relies on numerous mosquito-encoded host factors such as tissue receptors and immune regulators while also being attacked by restriction factors of the mosquito’s innate immune system¹. Characterization of these crucial *Anopheles*–*Plasmodium* interactions can enable the identification of malaria transmission-blocking targets. An advantage of targeting *Plasmodium* host factors, in contrast to restriction factors,

for malaria control strategies is the availability of multiple intervention methods. These include RNA interference (RNAi)-mediated gene silencing, CRISPR–Cas9-based gene editing, transmission-blocking vaccines (TBV) and small-molecule inhibitors².

Chaperones mediate the proper folding of proteins and the assembly of macromolecular structures, which can be broadly classified into the GroEL–GroES folding system and the thermosome–CCT (cytosolic chaperonin containing the peptide tail-less complex polypeptide 1) system. CCT is an ATP-dependent class II chaperonin that aids in the proper folding of actin, α -tubulin and β -tubulin for cytoskeletal assembly, with the help of the co-chaperone prefoldin (PFDN) complex^{3,4}. These macromolecular complexes have also been shown to be important

¹W. Harry Feinstone Department of Molecular Microbiology and Immunology, Bloomberg School of Public Health, Johns Hopkins University, Baltimore, MD, USA. ²Department of Entomology, Armed Forces Research Institute of Medical Sciences, Bangkok, Thailand. ³Present address: Department of Biomedical Sciences, Institute of Tropical Medicine Antwerp, Antwerp, Belgium. ✉e-mail: gdimopo1@jhu.edu

for *Plasmodium* invasion of the midgut epithelium^{5,6}. The PFDN complex comprises two alpha subunits, PFDN3 and PFDN5, and four beta subunits, PFDN1, PFDN2, PFDN4 and PFDN6, which together form a jellyfish-like structure with coiled-coil tentacles that determine substrate specificity during binding to non-native target proteins^{7–9} (Fig. 1a). The hexameric PFDN protein complex binds co-translationally to the unfolded proteins, aids in stabilizing the actin and tubulin subunits and forms a binary complex before interacting with CCT to form the ternary complex¹⁰. Actin and tubulin proteins are essential for cell division, motility, molecular transport, cytoskeletal stability and signal transduction, and influence *Plasmodium* infection¹¹. The PFDN-chaperonin complex has also been shown to play broader functions in protein homeostasis under normal and pathological conditions, and non-canonical functions have also been identified for individual subunits^{7,12}.

Plasmodium's major bottleneck in the mosquito is the traversal of the midgut epithelium, where ookinete invasion is influenced by a variety of mosquito agonistic and antagonistic proteins^{13–17}. The midgut epithelial actin–cytoskeleton reorganization and tubulin subunit folding, along with microtubule movement, are pivotal in determining successful invasion and infection^{5,18–20}. The microbiota in the ingested blood meal will proliferate and prime an anti-*Plasmodium* immune response, including the thioester-domain-containing protein 1 (Tep1)-mediated complement system and other defence reactions, and it has to be controlled and contained in the midgut lumen to avoid systemic infection^{21–23}. Understanding these interactions is crucial for developing strategies to disrupt malaria transmission in the vector mosquito. Interestingly, different *Plasmodium* and *Anopheles* species combinations differ with regard to these interactions in terms of both host and restriction factors, and this diversity makes it difficult to develop universal transmission-blocking strategies that can function across all potential *Anopheles* and *Plasmodium* species pairings^{1,17,24,25}. The responses of midgut epithelial cells to ookinete invasion in different mosquito–parasite combinations show species-specific mechanisms²⁶.

Here we show that the PFDN–CCT/TriC (T-complex protein ring complex) chaperonin complex serves as a host factor system for multiple *Plasmodium* species in all tested *Anopheles* species. Interfering with the PFDN–CCT/TriC chaperonin complex results in a cascade of events, including compromised gut integrity and disrupted extracellular matrix organization. The increased gut permeability leads to bacterial leakage and systemic infection, ultimately augmenting antiplasmoidal defences and resulting in mosquito death. These processes also compromise the parasite's laminin-based immune evasion mechanism, enabling the primed immune system to attack it effectively.

The PFDN–chaperonin complex is required for infection in diverse *Anopheles*–*Plasmodium* species combinations

A comprehensive yeast two-hybrid screen to identify putative *Plasmodium falciparum* host and restriction factors²⁷, followed by RNAi-based screening of selected genes for influence on *Plasmodium* infection, identified *Anopheles gambiae* PFDN6 as a likely parasite host factor (Fig. 1b,c). RNAi-mediated depletion of *Pfdn6* (78.3% knock-down (KD) efficiency; Supplementary Table 1) by double-stranded RNA (dsRNA) injection 3 days before feeding on *P. falciparum* gametocytes via a standard membrane feeding assay (SMFA) significantly reduced oocyst load in the midgut by 2.9-fold (66% inhibition, $P = 0.0002$) at 8 days postinfection (dpi) compared with *Gfp* dsRNA-injected controls (Fig. 1b,c and Supplementary Tables 1 and 2). To determine whether the PFDN–CCT/TriC chaperonin complex acts as a *Plasmodium* host factor rather than PFDN6 having an independent host factor function, we individually silenced all six PFDN subunits (*pfdn1–6*) or *CCT subunit 4* (*CCT4*) genes and assessed the effect on mosquito permissiveness to parasite infection. The *CCT4* was selected because of its functional interaction with PFDN3 in *Saccharomyces cerevisiae*²⁸. Indeed, silencing

any of the six *Pfd* genes or *CCT4* (>70% KD efficiencies; Supplementary Table 1) similarly reduced infection intensity and prevalence significantly (Fig. 1d,e and Supplementary Table 2). Furthermore, co-silencing of one of the two alpha-type subunit genes, *Pfdn3*, with *Pfdn6* (one of the four beta-type subunit genes) showed no additive effect, confirming that host factor function operates via the PFDN–CCT/TriC complex, and not through independent functions of individual subunit(s) (Fig. 1f and Supplementary Table 2). Small oocysts, indicating retardation of sporogonic development, were observed in the *Pfdn6*-silenced mosquitoes (Fig. 1g,h). On the basis of these results, we continued our studies by targeting the PFDN6 subunit to inactivate the *Plasmodium* host factor activity of the PFDN–CCT/TriC chaperonin complex.

The high sequence homology of PFDN6 across mosquito species suggests a conserved function of the PFDN complex and its probable role as a host factor for *Plasmodium* in multiple *Anopheles* species (Fig. 1i and Supplementary Data 1). Indeed, *Pfdn6* silencing in *Anopheles stephensi* (an Asian malaria vector expanding into Africa) resulted in a significantly lower median of 17 versus 55 *P. falciparum* oocysts and a 17% decrease in infection prevalence compared with the *Gfp* dsRNA-injected control cohort at 8 dpi ($P < 0.0001$; Fig. 1j and Supplementary Table 2). To determine whether the PFDN–CCT/TriC chaperonin complex also plays a host factor role for the evolutionarily distant rodent malaria parasite *Plasmodium berghei*, we silenced the *A. gambiae* *Pfdn6* before feeding mosquitoes on a *P. berghei*-infected mouse and again observed a significant reduction in oocyst-level infection intensity and prevalence at 12 dpi ($P < 0.0001$ for both infection intensity and prevalence; Fig. 1k and Supplementary Table 2).

Next, we investigated the suitability of PFDN6 as a *Plasmodium* TBV target by generating a rabbit anti-PFDN6 polyclonal antibody (Washington Biotechnology) that was co-fed to *A. gambiae* along with a *P. falciparum* gametocyte-infected blood meal using SMFA (Fig. 2a). Ingestion of purified anti-PFDN6 polyclonal antibody (IgG) resulted in a significant decrease in parasite loads (either at the oocyst or sporozoite stage) compared with control cohorts fed on rabbit anti-GFP antibody (Fig. 2b,c, Extended Data Fig. 1a–d and Supplementary Table 2). Co-feeding *P. falciparum* gametocytes (either low or high gametocytaemia) with anti-PFDN6 at increasing titres (50 $\mu\text{g ml}^{-1}$ to 1,000 $\mu\text{g ml}^{-1}$) resulted in a potent suppression of parasite infection. At an unnaturally high infection level (0.1% gametocyte culture), anti-PFDN6 ingestion reduced oocyst loads by 28–68% at antibody concentrations of 100 $\mu\text{g ml}^{-1}$ to 400 $\mu\text{g ml}^{-1}$ (22–65% reduction in mean oocyst loads; Extended Data Fig. 1b and Supplementary Table 2). A significant number of smaller oocysts were also observed in the *Pfdn6*-silenced mosquitoes (Extended Data Fig. 1c,d). At a natural infection level commonly observed in field-caught mosquitoes, achieved by feeding mosquitoes on a tenfold lower gametocyte concentration (0.01% gametocytaemia), there was potent, dosage-dependent anti-PFDN6 antibody-mediated inhibition of *P. falciparum* infection intensity and prevalence of both oocyst and sporozoite stages^{29,30} (Fig. 2b,c and Supplementary Table 2). The decrease in mean oocyst loads ranged from 54% to 85% in mosquitoes fed on antibody concentrations of 50 $\mu\text{g ml}^{-1}$ to 400 μg (or 1,000 μg) ml^{-1} (Fig. 2b, Extended Data Fig. 1b and Supplementary Table 2). The reduction in median sporozoite loads ranged from 56% (33% in mean sporozoite loads) in mosquitoes fed on 50 $\mu\text{g ml}^{-1}$ antibody concentration to almost 100% (75% in mean sporozoite loads) in mosquitoes fed on a 400 μg (or 1,000 μg) ml^{-1} antibody concentration (Fig. 2c and Supplementary Table 2). These data suggest that transmission of human malaria parasites can be blocked entirely at antibody titres of 400 $\mu\text{g ml}^{-1}$ or greater. This inhibition level is comparable to that achieved with TBV candidate Pfs230 and Pfs25 antibodies³¹ and antibodies targeting mosquito proteins AgAPN1 and REP1 generated via a similar immunization method^{32,33}.

To investigate whether parasite blocking by the anti-PFDN6 antibody was mosquito species and/or *Plasmodium* species specific, we performed antibody-mediated parasite inhibition assays with the

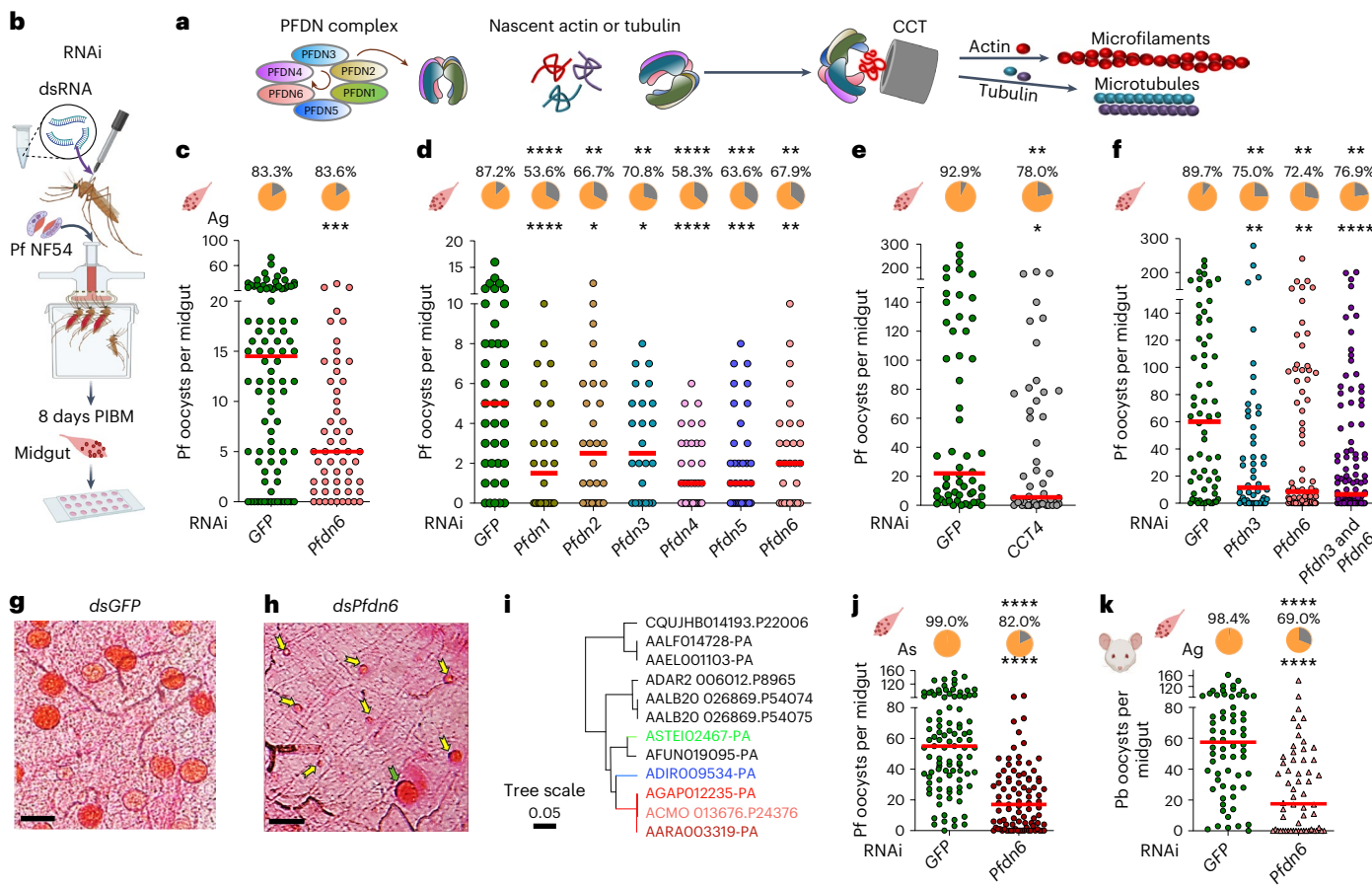


Fig. 1 | PFDN6 serves as a host factor for multiple malaria parasite species in multiple *Anopheles* species, and functions as a component of a heterohexameric protein complex known as PFDN–CCT/TRiC. **a**, PFDN–CCT/TRiC complex: six subunits of PFDN (with two alpha types (that is, PFDN3 and PFDN5 in blue) and four beta types (PFDN6 and PFDN1, PFDN2 and PFDN4, with corresponding colour codes)). The PFDN protein complex delivers nascent actin and tubulin to CCT/TrIC for the assembly of microtubules and microfilaments. **b**, RNAi-mediated gene silencing process and subsequent *P. falciparum* (Pf) infection assay. PIBM, post-infectious blood meal. **c**, *P. falciparum* oocyst-stage infection prevalence and intensity in *A. gambiae* (Ag) midguts after silencing of *Pfdn6* compared with the *Gfp*-RNAi control at 8 dpi. **d**, **e**, Significant decrease in *P. falciparum* oocyst loads after silencing each subunit of PFDN (**d**) and CCT subunit 4 (CCT4) (**e**). Detailed sequence alignments of *Pfdn* subunits and CCT4 are listed in Supplementary Data 2 and 3. **f**, Co-silencing of PFDN complex subunit genes *pfdn6* and *pfdn3* shows no additive effect on mosquito permissiveness to *P. falciparum* oocyst-stage infection.

g, **h**, Representative microscopic images of mercurochrome staining of midguts with mature large oocysts in the control *Gfp* dsRNA-injected group (**g**) and small oocysts (**h**, yellow arrows; green arrow, mature large oocyst). *n* = 20; scale bars, 75 μ m. **i**, Phylogenetic tree of PFDN6 in various mosquito species with the nodes of *A. gambiae* (red), *A. stephensi* (green) and *A. dirus* (blue) and others (sequence alignment details in Supplementary Data 1). **j**, **k**, *P. falciparum* oocyst-stage infection prevalence and intensity in the midgut of *A. stephensi* (As) at 8 dpi (**j**) and *P. berghei* infection in *A. gambiae* mosquitoes at 12 dpi (**k**). Each dot represents oocyst numbers in an individual mosquito (**c–f,j,k**), and the red line indicates the median. The small pie charts show infection prevalence. At least three replicates were included, and statistical significance was determined using the Mann–Whitney *U* test (two tailed) for infection intensity and Fisher's exact test for infection prevalence. **P* < 0.05; ***P* < 0.01; ****P* < 0.001; *****P* < 0.0001. Detailed statistical analysis and *P* values are provided in Supplementary Table 2. Panel **b** created with BioRender.com.

P. falciparum oocyst-stage infection. **g**, **h**, Representative microscopic images of mercurochrome staining of midguts with mature large oocysts in the control *Gfp* dsRNA-injected group (**g**) and small oocysts (**h**, yellow arrows; green arrow, mature large oocyst). *n* = 20; scale bars, 75 μ m. **i**, Phylogenetic tree of PFDN6 in various mosquito species with the nodes of *A. gambiae* (red), *A. stephensi* (green) and *A. dirus* (blue) and others (sequence alignment details in Supplementary Data 1). **j**, **k**, *P. falciparum* oocyst-stage infection prevalence and intensity in the midgut of *A. stephensi* (As) at 8 dpi (**j**) and *P. berghei* infection in *A. gambiae* mosquitoes at 12 dpi (**k**). Each dot represents oocyst numbers in an individual mosquito (**c–f,j,k**), and the red line indicates the median. The small pie charts show infection prevalence. At least three replicates were included, and statistical significance was determined using the Mann–Whitney *U* test (two tailed) for infection intensity and Fisher's exact test for infection prevalence. **P* < 0.05; ***P* < 0.01; ****P* < 0.001; *****P* < 0.0001. Detailed statistical analysis and *P* values are provided in Supplementary Table 2. Panel **b** created with BioRender.com.

major Asian malaria vector *A. stephensi* and a major Southeast Asian malaria vector, *Anopheles dirus* (from the forested zones of Myanmar, Thailand, Cambodia, Laos, Vietnam and China's Hainan Island), with *P. falciparum* and *Plasmodium vivax* infections, respectively. Given the high conservation of PFDN6 across mosquito species (Fig. 1*i* and Supplementary Data 1), we used the same *A. gambiae* anti-PFDN6 antibody for co-feeding and SMFA with various *Anopheles* and *Plasmodium* species. Co-feeding *A. stephensi* with *P. falciparum* gametocytes and the anti-PFDN6 antibody resulted in profound 56% suppression of mean oocyst infection intensity (*P* < 0.0001; Fig. 2*d* and Supplementary Table 2). Similarly, co-feeding *A. dirus* with *P. vivax*-infected donor blood and the anti-PFDN6 antibody resulted in a significant 76% suppression of mean oocyst load (*P* = 0.0001; Fig. 2*e* and Supplementary Table 2).

To determine, as a proof of principle, whether PFDN6 can serve as a malaria TBV candidate, we used a rodent malaria infection model involving immunization, infection and mosquito transmission studies

(Fig. 2*f*). Five mice received subcutaneous injections of 10 μ g PFDN6 recombinant protein (rPFDN6) in Freund's adjuvant at 2-week intervals with two boosters (Extended Data Fig. 1*e*) according to established protocols^{34,35}. Controls received recombinant GFP injections using the same protocol. Two weeks after the second booster, three out of five immunized mice showed high antibody titres as determined by ELISA (Extended Data Fig. 1*f*) and were infected with *P. berghei*. When parasitaemia and gametocytaemia reached 8% and 2.5%, respectively, at 2–3 dpi, the mice were used for mosquito infection assays. Mosquitoes fed on the PFDN6-immunized mice showed a significantly lower oocyst infection intensity and prevalence compared with those fed on GFP-immunized mice at 12 dpi, further indicating that PFDN6 is a potent candidate Plasmodium TBV target (94% and 75% inhibition of median or mean oocyst loads, respectively, *P* < 0.0001; *P* < 0.01 on infection prevalence; Fig. 2*f* and Supplementary Table 2). These results, together with those presented above, show that PFDN6, and presumably other members of the PFDN–CCT/TRiC chaperonin complex, are conserved

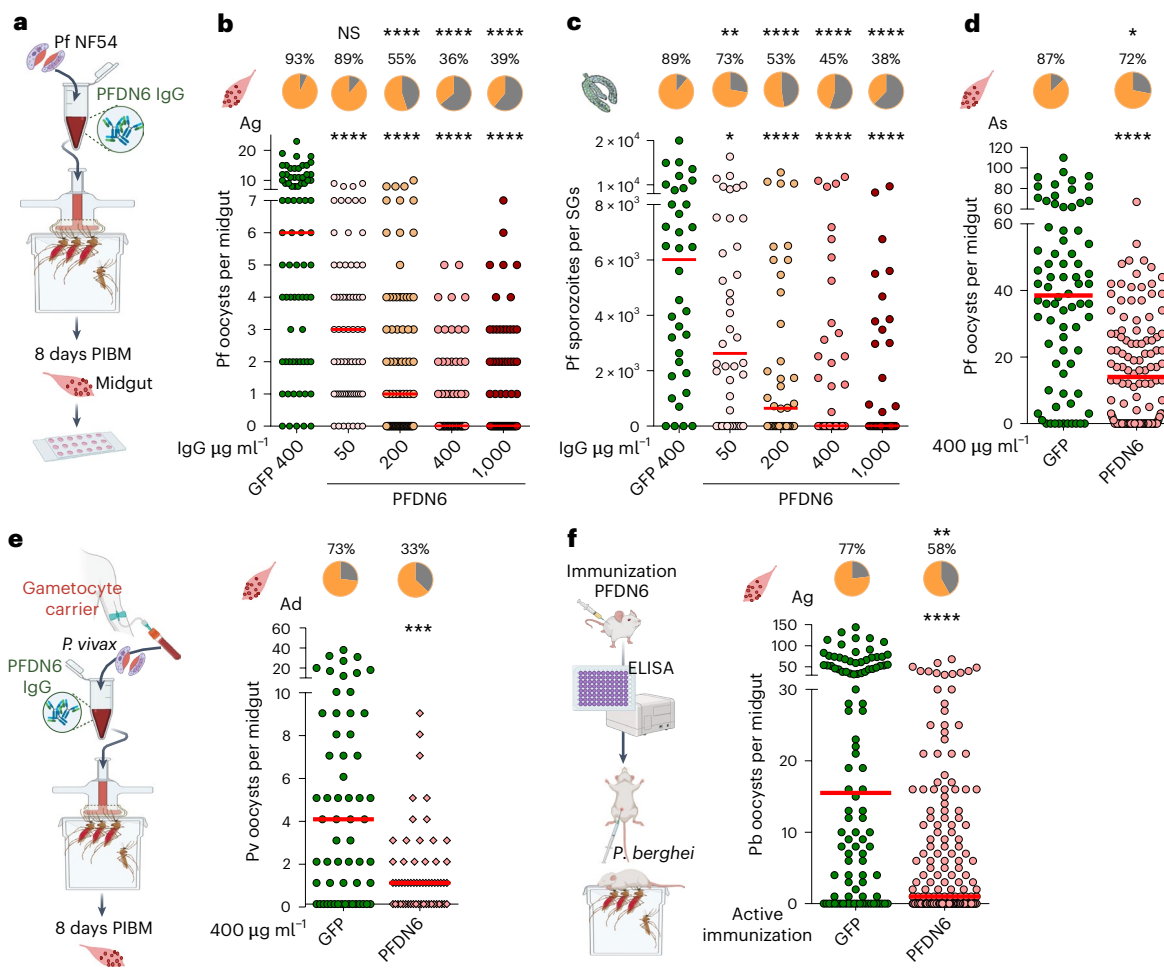


Fig. 2 | Anti-PFDN6 antibody blocks a broad spectrum of *Plasmodium* species in diverse *Anopheles* mosquito vectors. a, Overview of the co-feeding of *P. falciparum* (Pf) gametocytes with anti-PFDN6 antibody, along with infection phenotype assays. **b-d**, Co-feeding of anti-PFDN6 antibody and *P. falciparum* gametocytes reduces the number of oocysts at 7–8 dpi in *A. gambiae* (**b**) and *A. stephensi* (**d**), and the number of sporozoites in *A. gambiae* salivary glands (SGs) at 14 dpi (**c**). **e**, Left: overview of *P. vivax* (Pv) infection assay using blood from gametocyte carriers through an artificial membrane feeding system. Right: co-feeding of anti-PFDN6 antibody and Pv-infected blood reduces the number of oocysts at 8 dpi in *A. dirus*. **f**, Left: active immunization assay involving mouse immunization with recombinant PFDN6 protein and subsequent *P. berghei* (Pb)

infection assay. Right: blood-feeding *A. gambiae* on Pb-infected mice that had been immunized with recombinant PFDN6 reduces the number of oocysts at 12 dpi. Each data point represents the number of oocysts (**b,d,e,f**) or sporozoites in an individual mosquito's salivary glands (**c**), and the red line indicates the median number. Small pie charts indicate infection prevalence. At least three replicates were included, and statistical significance was determined using the Mann-Whitney *U* test (two tailed) for infection intensity and Fisher's exact test for infection prevalence. * $P < 0.05$; ** $P < 0.01$; *** $P < 0.001$; **** $P < 0.0001$. NS, not significant. Detailed statistical analysis and numbers are provided in Supplementary Table 2. Panels **a**, **e** and **f** created with BioRender.com.

transmission-blocking targets and suitable for TBV development across *Anopheles* and *Plasmodium* species.

PFDN plays its host factor function for epithelium ookinete and early oocyst stages

To pinpoint the specific pre-oocyst developmental stage of *Plasmodium* affected by the host factor function of PFDN, we performed co-feeding assays with anti-PFDN6 antibody and *P. falciparum* gametocytes and determined the numbers of ookinetes after ingestion in the *A. gambiae* midgut lumen and epithelial cells at 24 h, as well as oocyst numbers on the basal side of the midgut epithelium at 36 h and 8 days (Extended Data Fig. 2a). No significant difference in ookinete numbers in the midgut lumen and only a slight difference in the epithelium were observed at 24 h between the anti-PFDN6 and control (anti-GFP) antibody-treated groups (Extended Data Fig. 2b,c and Supplementary Table 2), but a significantly decreased oocyst load was observed at both 36 h ($P < 0.0001$; Extended Data Fig. 2d and Supplementary Table 2) and 8 dpi (Fig. 2b, Extended Data Fig. 1b and Supplementary Table 2). To assess the spatial

specificity of the anti-PFDN6 antibody-mediated parasite suppression, we injected the antibody into the haemolymph of adult female mosquitoes 2 days before they were fed *P. falciparum* gametocytes (Extended Data Fig. 2a). This treatment resulted in significantly reduced oocyst numbers ($P = 0.0022$; Extended Data Fig. 2e and Supplementary Table 2), suggesting that the blocking activity of the antibody may be exerted on the basal region of the midgut epithelium. These results indicate that PFDN host factor function is exerted upon ookinete egress and oocyst formation on the basal side of the epithelium beneath the basal lamina.

Next, we investigated whether PFDN6 was co-localized with the invading parasites in the midgut epithelium. To evaluate this, we examined mosquito midgut epithelia by confocal microscopy at 24 h to 28 h after feeding the mosquitoes *P. falciparum* gametocytes, using the anti-PFDN6 antibody together with a *P. falciparum*-specific anti-Pfs25 antibody. We did not observe co-localization of PFDN6 with the parasite in the epithelial cells; instead, its distribution largely overlapped with that of actin (Extended Data Fig. 3a,b), suggesting that PFDN6 is not

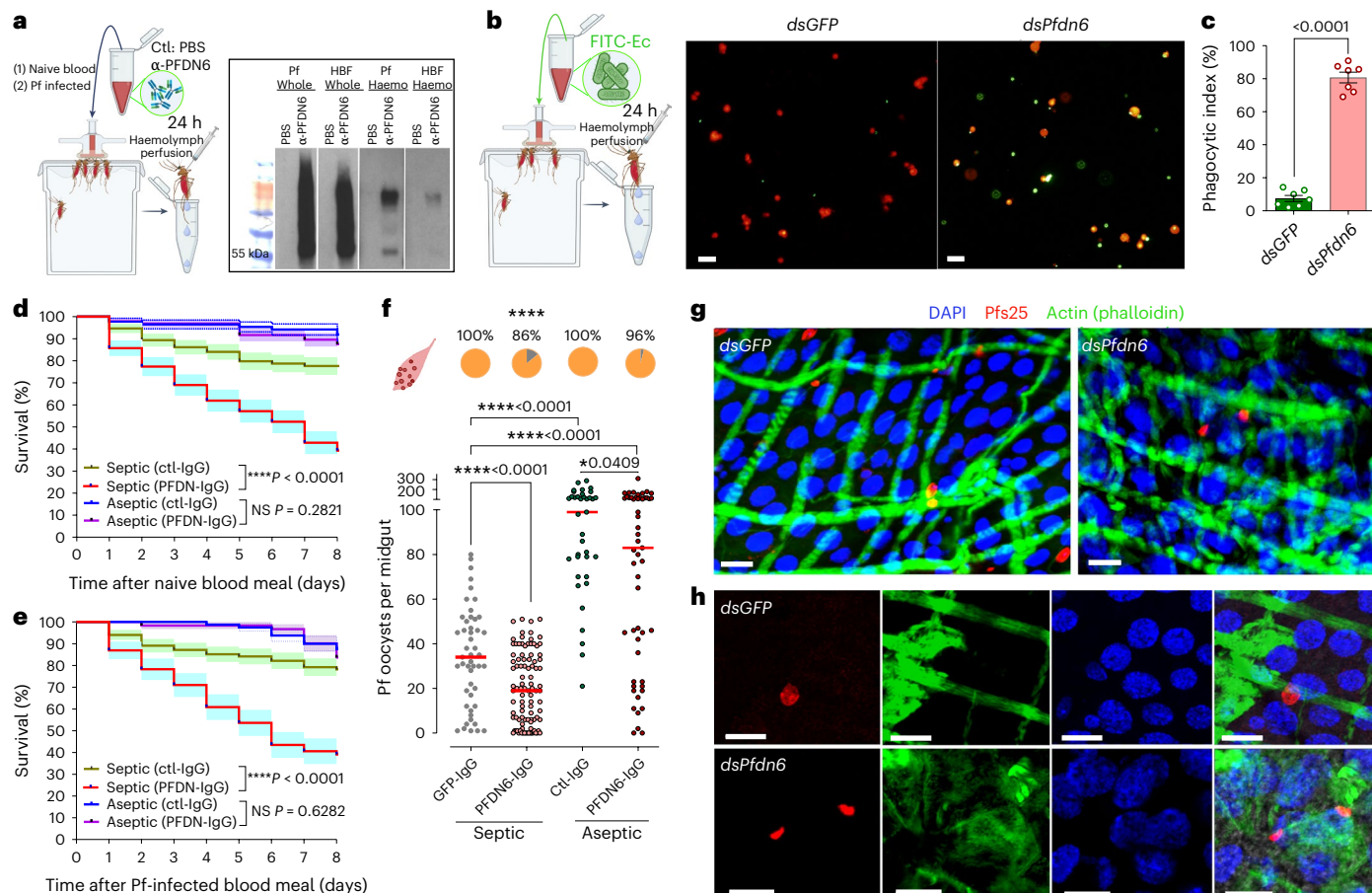


Fig. 3 | Disruption of the PF DN complex through RNAi gene silencing of *Pfdn6* or anti-PFDN6 co-feeding compromises the integrity of the midgut physical barrier. **a**, Left: overview of haemolymph perfusion from mosquitoes co-fed with anti-PFDN6 and naive blood or *P. falciparum* (Pf) gametocyte blood mix 24 h PBM. Right: western blot analysis showing greater diffusion of anti-PFDN6 into the haemolymph of mosquitoes after the Pf-infected blood meal. PBS, control PBS-fed mosquitoes; α-PFDN6, anti-PFDN6 fed; haemo, haemolymph; whole, whole mosquitoes; Pf, Pf blood fed; HBF, naive human blood fed. Left lane: SeeBlue Plus2 pre-stained protein standard. Rabbit anti-HRP to detect the antibody. Protein loading, 10 µg total protein. $n = 3$ for each treatment. **b**, Left: collection of haemolymph from mosquitoes co-fed with blood and FITC-labelled *E. coli* (Ec) bacteria. Right: the representative fluorescence microscope images of haemolymph from the dsGFP control or *Pfdn6*-silenced (*dsPfdn6*) mosquitoes ($n = 20$). Green, bacteria; red, haemocytes. **c**, Phagocytic index showing greater bacterial perfusion in *dsPfdn6* mosquitoes, with significance calculated by Student's *t*-test (two tailed); $n = 7$, with each circle representing one replicate and bar with mean ± s.e. shown. **d,e**, Survival curves of mosquitoes co-fed with

control (ctl-IgG) or anti-PFDN6 (PFDN-IgG) antibodies and naive blood (**d**) or Pf-infected blood (**e**) with (septic) or without (aseptic) natural microbiota. Three biological replicates with at least 35 blood-fed mosquitoes per group. Kaplan–Meier survival analysis (two tailed) determined significance along with the shaded error bars representing the confidence intervals (95%). **f**, Significant reduction of oocyst loads at 8 dpi in the presence of natural microbiota in the leaky gut, and antibiotic treatment resulted in a less pronounced reduction in oocyst loads. Each dot represents oocyst loads in an individual mosquito midgut, with the median shown in the red line. * $P < 0.05$; *** $P < 0.0001$; Mann–Whitney *U* test (two tailed). Pie chart: infection prevalence, significance by Fisher's exact test. Three biological replicates are shown. Details are given in Supplementary Table 2. **g,h**, Representative confocal microscopy images of *P. falciparum* ookinete and oocysts shown at low (**g**) and high (**h**) magnifications, with anti-Pfs25 (Alexa-568, red), actin cytoskeleton (Alexa-488-phalloidin, green) and nuclei (blue). The midgut physical barrier is less integrated during ookinete invasion in *dsPfdn6* mosquitoes compared with controls (dsGFP). Scale bars, 10 µm; $n = 20$. Panels **a** and **b** created with BioRender.com.

exerting its parasite host factor activity through direct interaction or close association with the parasite. We also did not observe parasite infection-inducible or tissue-specific expression of *Pfdn6* (Extended Data Fig. 3c,d), showing that PF DN is not transcriptionally responsive to parasite infection.

Disruption of the PF DN–chaperonin complex compromises the integrity of the midgut physical barrier and shortens the mosquito lifespan

We attempted to generate a CRISPR–Cas9-mediated *A. gambiae* *Pfdn6* knockout (KO) mutant (Extended Data Fig. 4), but the somatic *Pfdn6* KO mosquitoes showed pre-adult lethality, probably owing to severe distortion of the cytoskeletal structure and gut integrity (Extended Data Fig. 4g). A PF DN co-immunoprecipitation (co-IP) assay further supported this function for mosquito PF DN (Extended Data Fig. 5 and

Supplementary Table 3), identifying *A. gambiae* actin and tubulin proteins²⁷, along with several extracellular matrix proteins (Extended Data Fig. 5 and Supplementary Table 3). These results align with previous studies showing that the PF DN–CCT/TriC chaperonin complex regulates actin and tubulin polymerization, crucial for maintaining cell and extracellular matrix integrity^{7,8,36,37}.

On the basis of these findings, and the fact that PF DN appears to function as a host factor for *Plasmodium* during ookinete egress and early oocyst development, we hypothesized that the PF DN–CCT/TriC chaperonin complex's host factor role is linked to midgut integrity and/or extracellular matrix organization. To test this, we investigated midgut epithelial barrier integrity during ookinete traversal of the epithelium after PF DN disruption through either RNAi gene silencing or co-feeding of anti-PF DN antibodies. Following co-feeding of mosquitoes with the anti-PF DN antibody and either naive (human

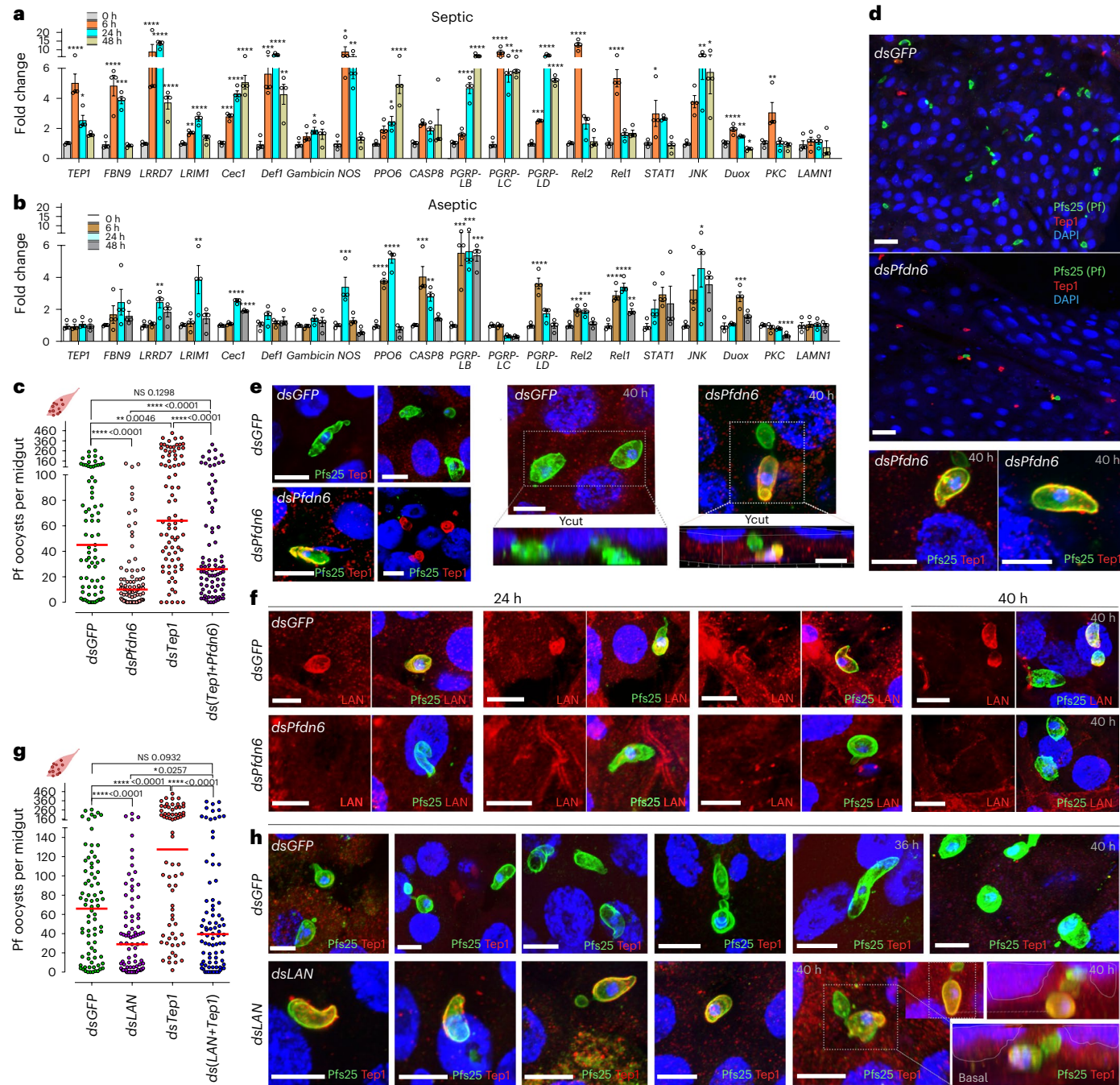


Fig. 4 | Disrupting the PFDN complex causes a leaky gut, triggering immune priming through microbiota, including Tep1, enabling immune factors to access *P. falciparum* parasites and block them effectively in the absence of a laminin coating. **a,b**, qRT-PCR analysis of immune and damage-related gene expression in midguts 6 h, 24 h and 48 h PBM, showing significant upregulation in mosquitoes with natural microbiota (septic; **a**) compared with antibiotic-treated mosquitoes (aseptic; **b**) in the *Pfdn6*-silenced (*dsPfdn6*) mosquitoes compared with the controls (*dsGFP*). The housekeeping ribosomal S7 gene was used as a reference for normalization, with the details of each gene in Supplementary Table 1. One-way ANOVA with Dunnett's post hoc test determined significance. $n = 4$, with each circle representing one replicate, and mean \pm s.e. is shown. * $P < 0.05$; ** $P < 0.01$; *** $P < 0.001$; **** $P < 0.0001$. Exact P values are given in Source Data. **c,g**, *P. falciparum* (Pf) oocyst infection intensity in midguts after silencing *Pfdn6* (*dsPfdn6*), *Tep1* (*dsTep1*) or laminin (*dsLAN*), or co-silencing either the combinations as (*ds(Tep1+Pfdn6)*) or (*ds(LAN+Tep1)*). Each data point represents

the oocyst count per mosquito midgut, with the red line indicating the median. Three replicates are shown. * $P < 0.05$; ** $P < 0.01$; *** $P < 0.001$; **** $P < 0.0001$; Mann–Whitney U test (two tailed). *Laminin* silencing (**g**) significantly decreased oocyst loads similar to *Pfdn6* silencing (**c**). Statistical analysis and infection prevalence are given in Supplementary Table 2. **d,e,f,h**, Confocal microscopy of midguts at 24–28 h and 36–40 h postinfection. More *Tep1* (red) co-localized with ookinetes or early oocysts (*Pfs25*, green) in *Pfdn6*-silenced mosquitoes (*dsPfdn6*) than controls (*dsGFP*) (**d,e**). More laminin (LAN, red) was found on invading ookinetes or oocysts in controls (*dsGFP*) than in the leaky gut (*dsPfdn6*) (**f**). More *Tep1* co-localized with ookinetes or oocysts when laminin was disrupted (*dsLAN*) than in controls (*dsGFP*) (**h**). Anti-*Pfs25* (green), *P. falciparum* ookinetes and oocysts; DAPI (blue), epithelial nuclei; anti-*Tep1* or anti-laminin (red), respective proteins. Scale bars, 20 μm (**d**) and 5 μm (**e,f,h**). The default time point is 24–28 h, in which no specific label was indicated. Confocal analysis included at least 20 midguts per group, with fluorescence quantification in Supplementary Tables 4–6.

blood fed (HBF)) or gametocyte-containing blood (Pf), we perfused the haemolymph and detected the presence of anti-PFDN6 antibody in the haemolymph of both groups (Fig. 3a). However, the concentration of anti-PFDN6 was over ten times higher in the haemolymph of infected mosquitoes (Pf haemo) compared with naive mosquitoes (HBF haemo), as quantified by ImageJ. These results suggest that antibody diffusion through the midgut epithelium is prompted by the physical distension of the midgut caused by the blood meal^{38–40} and is further facilitated by ookinete invasion, probably through increased permeability caused by the invasion process and the accompanying injury. The mosquito midgut contains a diverse microbiota, predominantly Gram-negative bacteria, and its integrity is essential to prevent lethal systemic infection from bacterial leakage into the haemolymph^{23,41}. Silencing *Pfdn6* followed by feeding on a blood meal with a suspension of FITC-labelled *Escherichia coli* resulted in significant bacterial leakage into the haemolymph; by contrast, the haemolymph of the *Gfp* dsRNA-treated controls barely contained any green fluorescence bacteria at 24 h after feeding (Fig. 3b). The *Pfdn6*-silenced and *E. coli*-fed mosquitoes also showed an eightfold increase in the haemocyte phagocytic index, indicating a systemic bacterial infection ($P < 0.0001$; Fig. 3c).

When non-antibiotic-treated (referred to as septic) mosquitoes from the insectary were given either a naive or a *P.falciparum*-infected blood meal alongside anti-PFDN6 antibody (PFDN6-IgG) or control antibody (ctl-IgG), there was a significant proliferation of the natural microbiota in the midgut of both mosquito groups ($P = 0.0433$; Extended Data Fig. 6a). This proliferation led to the leakage of midgut microbiota into the haemolymph, resulting in significantly higher mortality rates of mosquitoes fed with PFDN6-IgG compared with those fed with ctl-IgG (refer to septic ctl-IgG versus PFDN-IgG in Fig. 3d,e). However, when mosquitoes were treated with antibiotics (refer to aseptic) to suppress the midgut microbiota, those fed with PFDN6-IgG showed no difference in mortality compared with the controls (Fig. 3d,e). The leaky gut, coupled with bacterial proliferation, blocked the parasites at a pre-oocyst stage, and antibiotic treatment partially alleviated this hindrance, resulting in a less pronounced reduction in oocyst loads after suppressing the microbiota ($P < 0.0001$ in the septic mosquitoes compared with $P < 0.05$ in the aseptic mosquitoes; Fig. 3f and Supplementary Table 2). However, in the absence of a blood meal, there was no difference in mosquito survival between those given a sugar meal supplemented with PFDN6-IgG versus control IgG, nor between *Pfdn6*-silenced mosquitoes and those *Gfp* dsRNA-treated controls (Extended Data Fig. 6b–f). At 36 h after the mosquitoes were fed on *P. falciparum* gametocytes (during ookinete invasion and early oocyst formation), confocal microscopy examination of the F-actin-stained midgut epithelium of *Pfdn6*-silenced mosquitoes showed a less organized and structured actin cytoskeleton by phalloidin staining compared with *Gfp* dsRNA-injected controls (Fig. 3g,h). No such difference was found in *Pfdn6*-silenced mosquito midguts maintained on a sugar meal (Extended Data Fig. 6g,h). These data further suggest that the PFDN–CCT/TriC chaperonin complex is crucial for maintaining the integrity of the midgut's physical barrier, particularly after the blood meal, when the barrier is compromised through physical distention^{38,39}.

The microbial leakage upon midgut barrier disruption triggers anti-*Plasmodium* immune responses

We have previously shown that the *A. gambiae* midgut microbiota primes the innate immune system, resulting in a more potent anti-*Plasmodium* response^{23,24}. As a result, we hypothesized that the *Pfdn6* silencing-mediated disruption of gut epithelial integrity, which results in significant bacteria leakage into the haemolymph, would trigger a stronger-than-normal immune priming against *Plasmodium*. To address this hypothesis, we compared the mRNA abundance of multiple key anti-*Plasmodium* immune factors in *Pfdn6*-silenced and *Gfp* dsRNA-treated controls under both septic and aseptic conditions

at 6 h, 24 h and 48 h after a blood meal (PBM) (see the description of the genes in Supplementary Table 1). Indeed, under septic conditions, the genes encoding anti-*Plasmodium* factors *Tep1* (ref. 13), fibrinogen-related-protein 9 (FBN9)⁴² and leucine-rich immune protein 7 (LRRD7)^{24,43} showed 5-, 4.8- and 10-fold higher mRNA levels, respectively, at 6 h PBM in *Pfdn6*-silenced septic mosquitoes compared with the control. However, no significant difference was observed between the two groups under aseptic conditions (Fig. 4a,b). Several pattern recognition receptor (PRR) genes and genes related to damage and repair, such as *Nitric oxide synthase (NOS)*, *Protein Kinase C (PKC)*, *Peptidoglycan Recognition Proteins (PGRP-LC, PGRP-LD)*, and anti-microbial peptides *Cecropin 1 (Cec1)* and *Defensin 1 (Def1)*, and the IMD-pathway NF-κB transcription factor gene *Rel2*, were strongly upregulated, indicating that the leakage of microorganisms into the haemolymph caused by PFDN–CCT/TriC chaperonin complex disruption in the midgut potentiates the mosquitoes' immune defence against *Plasmodium*. In addition, genes associated with damage response (including *NOS*, *Caspase 8 (CASP8)*, *Prophenoloxidase 6 (PPO6)*, *STAT* and *JNK*) showed significant upregulation, irrespective of antibiotic treatment, aligning with our leaky gut hypothesis. Furthermore, immune pathway-related genes, including *PGRP-LB*, *PGRP-LD* and *Rel2*, were upregulated in the aseptic condition, probably attributed to the persistence of pathogen-associated molecular patterns from deceased bacteria after antibiotic treatment. This explains why, following the removal of the microbiota, the reduction in oocyst loads could be only partially alleviated (Fig. 3f), probably attributed to the sustained expression of immune and defence genes.

A disrupted midgut barrier probably increases parasite accessibility to haemolymph-derived immune factors, such as *Tep1*, a key anti-*Plasmodium* immune factor that mediates killing through direct parasite interaction^{13,21,44}. This mechanism requires parasite exposure during midgut traversal and lodging under the basal lamina to form an oocyst. Therefore, we silenced *Pfdn6* and *Tep1* alone or together to see whether *Pfdn6* silencing would influence the *Tep1*-mediated killing of *Plasmodium*. Silencing *Tep1* or *Pfdn6* alone resulted in significantly increased or decreased, respectively, permissiveness to parasite infection. However, co-silencing of both factors showed the same infection phenotype as that of the *Gfp* dsRNA-injected controls, as the effects of silencing each factor counterbalanced each other (Fig. 4c and Supplementary Table 2; $P = 0.1298$). This result suggests that the PFDN–CCT/TriC chaperonin complex exerts its *Plasmodium* host factor role by making the parasite less accessible to *Tep1* and possibly other immune factors. Indeed, our confocal microscopy studies showed that in the *Pfdn6*-silenced mosquito midguts, a significantly larger proportion of ookinetes that had traversed and egressed the midgut were co-localized with *Tep1* under the basal lamina, compared with *Gfp* dsRNA-injected controls (Fig. 4d,e and Supplementary Table 4). Interestingly, we found that the ookinetes were covered with *Tep1* as soon as they egressed the midgut epithelial cells on the basal side (Fig. 4e, y section, oonikete in the *Pfdn6*-silenced group).

A diminished laminin coating upon PFDN–chaperonin complex disruption facilitates parasite targeting by the *Tep1* complement factor

Our PFDN6 co-IP data indicated a possible interaction between the PFDN complex and laminin (Extended Data Fig. 5 and Supplementary Table 3), a basal lamina-associated parasite host factor crucial for the development of *P. berghei* ookinetes into early oocysts^{45–48}. RNAi-mediated silencing of *A. gambiae* laminin (*LANB2*, AGAP007629) upon infection with *P. falciparum* resulted in a significant decrease in oocyst numbers in the mosquito midguts as compared with the *Gfp* dsRNA-treated controls (Fig. 4g and Supplementary Table 2; 74% inhibition, $P < 0.0001$). Laminin has been shown to coat ookinetes and early oocysts, a feature that has been proposed as an immune-evasive mechanism shielding the parasite from the mosquito's immune system^{45,48,49}.

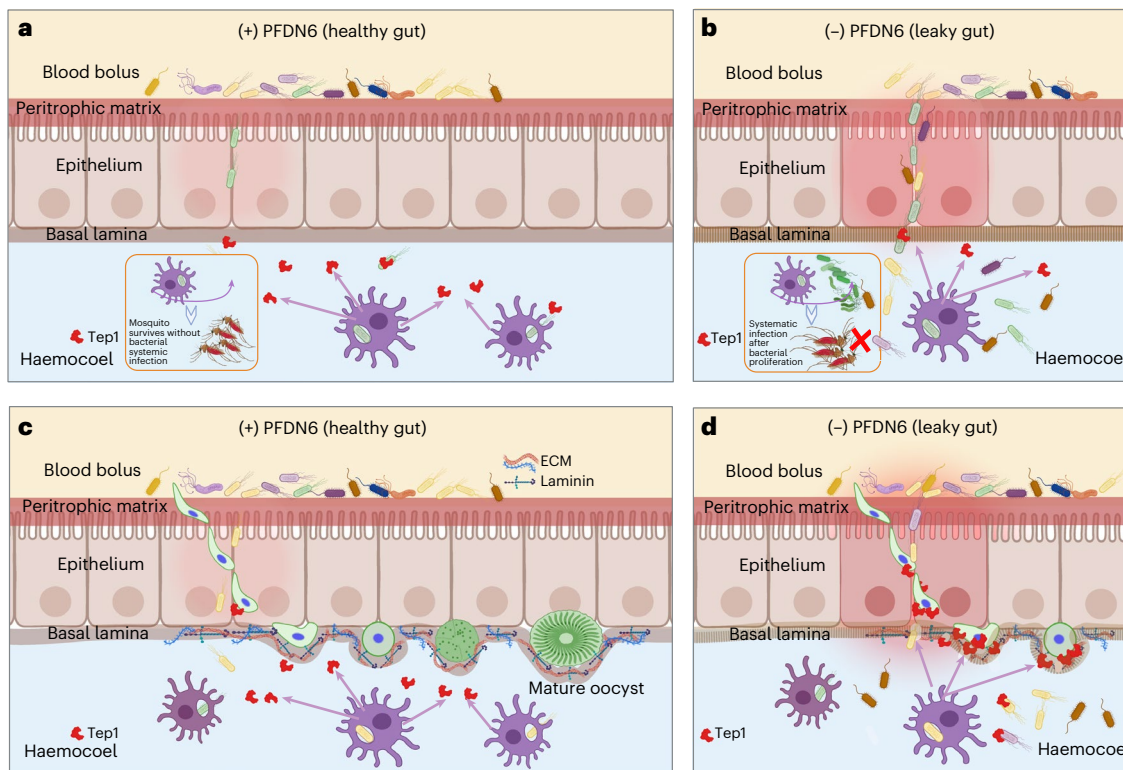


Fig. 5 | A proposed model illustrates that the disruption of the *Anopheles* PFDN–chaperonin complex leads to a leaky gut, which can either result in mosquito mortality due to bacterial proliferation or hinder the malaria parasite through microorganism-mediated immune priming. This disruption also facilitates the access of mosquito immune factors to the parasites, particularly in the absence of a laminin coating on the midgut basal lamina. **a,c**, In a healthy gut, when the midgut barrier remains intact after blood-meal-induced bacterial proliferation or during ookinete invasion of the midgut epithelial cells, the intact midgut protects mosquitoes from systemic infection (**a**), and the laminin coating provides protection for the ookinete, shielding it from exposure

to humoral immune factors, including Tep1 (**c**). Consequently, the ookinetes can successfully develop into mature oocysts on the gut basal lamina (**c**). **b,d**, In a leaky gut, disruption of the PFDN complex leads to the proliferation of natural microbiota in the mosquito midgut and systemic infection as microorganisms leak into the haemolymph, shortening the lifespan of the mosquitoes (**b**). This sequence of events initiates a natural microbiota-mediated immune priming response, disrupting the parasite's laminin-based immune evasion mechanism (**d**). Subsequently, this compromised defence allows unhindered access to anti-*Plasmodium* humoral immune factors, facilitating an effective attack against the parasites (**d**). Figure created with BioRender.com.

Our assays also showed that ookinetes and early oocysts at the basal side of the midgut are coated with laminin, and this coating was compromised when PFDN6 was depleted by RNAi-mediated gene silencing (Fig. 4f and Supplementary Table 5). Similarly, mosquitoes fed on the anti-PFDN6 antibody together with *P.falciparum* gametocytes did not show strong co-localization of laminin with ookinetes and early oocysts at 36 h after ingestion, whereas control mosquitoes did (Extended Data Fig. 7). These results underscore the pivotal role of PFDN in forming the protective laminin coating of the parasite. To further validate the hypothesis that the laminin coating protects parasites from Tep1 attack, we silenced *LAN* and *Tep1*, individually and together, upon *P.falciparum* infection. Co-silencing resulted in an infection phenotype comparable to that of *Gfp* dsRNA-injected controls, indicating a negation of the silencing effects observed individually (Fig. 4g and Supplementary Table 2). Confocal microscopy studies of *LAN*-silenced and *Gfp* dsRNA-injected controls showed that laminin prevented the Tep1-mediated attack against the ookinetes; in the absence of laminin, Tep1 strongly co-localized with the ookinetes and early oocysts (Fig. 4h and Supplementary Table 6).

Discussion

Here we show that the disruption of the PFDN–chaperonin complex in various anopheline mosquitoes leads to a condition that resembles the human leaky gut syndrome, which is responsible for a plethora of illnesses³⁶ (Fig. 5). This condition can hinder the transmission of multiple *Plasmodium* species in various *Anopheles*

mosquitoes owing to microorganism-mediated immune priming, and loss of laminin-dependent immune evasion that exposes *Plasmodium* to humoral immune factors such as the Tep1 complement system. This observation partially agrees with a previous study, which found that physical distension of the mosquito midgut from an additional blood meal compromises the integrity of the basal lamina, thereby increasing the exposure of *P. berghei* (but not *P. falciparum*) parasites to the mosquito complement system³⁹. This discrepancy is probably attributable to the intricate interplay between mosquito complement antiplasmoidal responses and cellular immunity²¹. An infection phenotype comprising smaller oocysts is similar to that when the parasite-protective c-type lectin 4 (CTL4) is inhibited and, therefore, further supports a loss of parasite immune-evasive ability upon PFDN–chaperonin complex disruption, exposing *Plasmodium* to the complement system and phenoloxidases⁵⁰. The leaky gut and resulting systemic bacterial infection also reduced the mosquito's lifespan (Fig. 5). Midgut epithelial integrity has also been shown to be essential for mosquito viability by a previous study in which inhibition of stearoyl-CoA desaturase resulted in a dramatic leakage of blood into the haemolymph and rapid death upon a blood meal, albeit by a different mechanism than PFDN–chaperonin targeting⁵¹.

Anti-PFDN6 antibody co-feeding assays resulted in a similar infection phenotype to RNAi-mediated *pfdn6* depletion, leading to transmission blocking of *P.falciparum*, *P.vivax* or *P.berghei* in *A.gambiae*, *A.stephensi* and *A.dirus* malaria vectors. An interesting feature is the ability of ingested antibodies to impede cytosolic PFDN;

a well-documented and published phenomenon^{37–39}. Blood feeding, coupled with ensuing infections, induces gut epithelium damage that facilitates the infiltration of antibodies into and across these cells. Indeed, our observations revealed the perfusion of antibodies into the mosquito haemolymph (Fig. 3a), and western blot analysis identified PFDN6 protein in haemocyte-free haemolymph (Extended Data Fig. 8). A major challenge in developing a TBV targeting the mosquito PFDN complex is its high sequence homology with human PFDN, raising concerns about cross-reactivity, autoimmune risks and host tissue damage. Addressing this requires strategies to enhance antigen specificity, such as epitope mapping or engineering mosquito-PFDN-specific variants, to minimize autoimmune effects while retaining efficacy. To gain some insight into the suitability of the PFDN–CCT/TriC chaperonin complex for TBV development, we investigated whether PFDN6 contained putative unique peptide epitopes that could alleviate concerns for off-target effects and induction of autoantibodies. Preliminary in silico analysis identified a promising unique B cell epitope for *A. gambiae* PFDN6 with no significant or low homology to human PFDN, suitable for vaccine development (Extended Data Figs. 9 and 10). Future work should focus on identifying and evaluating unique mosquito peptide epitopes from several PFDN–CCT/TriC chaperonin complex-associated proteins that can be efficiently targeted to destabilize the mosquito midgut epithelial barrier, thereby blocking parasite transmission and killing the vector. In addition, a multivalent vaccine targeting several PFDN–CCT/TriC chaperonin complex epitopes could help mitigate the potential selective pressure exerted by a mosquito-killing vaccine. Furthermore, the PFDN–CCT/TriC chaperonin complex could also be explored for conditional genetic inactivation in mosquito populations through a gene-drive mechanism for malaria control^{2,52–54}.

While the PFDN–chaperonin complex has been shown to play essential roles in both archaea and eukaryotes, it remains relatively understudied, especially concerning its function in infections⁷⁸. Our study furthers our knowledge of the biology of the PFDN–chaperonin complex in the context of epithelial integrity and host–pathogen interactions.

In summary, we show here that the role of the PFDN–CCT/TriC chaperonin complex *Plasmodium* host factor is based on maintaining midgut epithelial and extracellular matrix and basal lamina integrity that (1) limits the leakage of midgut microbiota into the haemolymph, where it can prime anti-*Plasmodium* immunity; (2) enables the parasite-protective coating with laminin; and (3) limits the attack by Tep1 and other potential immune factors on the invading ookinetes, possibly through the observed laminin coating (Fig. 5). Notably, the PFDN–CCT/TriC chaperonin complex represents a versatile malaria transmission-blocking target comprising over 10 possible (7 confirmed) *Anopheles* host factors for multiple malaria parasite species. Disruption of the PFDN–CCT/TriC chaperonin complex resulted in compromised fitness and reduced longevity of mosquitoes owing to bacterial leakage from the midgut into the haemolymph and systemic infection, further underscoring its multifaceted significance in malaria transmission control. These findings highlight the potential of the PFDN–CCT/TriC chaperonin complex as a promising target for intervention strategies to interrupt the transmission of multiple malaria parasite species in a broad spectrum of anopheline vectors.

Methods

Ethics

This study was carried out in strict accordance with the recommendations in the Guide for the Care and Use of Laboratory Animals of the National Institutes of Health. The protocol was approved by the Animal Care and Use Committee of Johns Hopkins University (permit number MO15H144 for regular blood feeding and *P. berghei* infection, and MO128H76 for mice immunization with recombinant proteins). Eight-week-old Female Swiss Webster mice were used for all the assays as indicated and housed in the Johns Hopkins School of Public Health

animal facility. Rabbit immunizations and antiserum collections were performed commercially by Washington Biotechnology, and as such, the animal protocol is unavailable. Commercial anonymous human blood (Interstate Blood Bank) was used for *P. falciparum* cultures and mosquito feeding, and informed consent was therefore not applicable. *P. vivax*-infected blood was collected from patients infected with malaria who were reporting to malaria clinics operated by the Thailand Ministry of Public Health in Tak Province (protocol WRAIR#1949B). Both the Walter Reed Army Institute of Research Institutional Review Board and the Ethical Review Committee for Research in Human Subjects, Ministry of Public Health, Thailand, have reviewed and approved the study protocol (WRAIR#1949B). Informed consent and permission were obtained from the participants before *P. vivax* blood samples were collected.

Mosquito rearing

A. gambiae Keele strain, *A. stephensi* Liston strain and *A. dirus* AFRIMS strain were maintained on a 10% sucrose solution with a 12-h day–night cycle at 27 °C and 80% humidity.

Total RNA preparation and qRT-PCR

Total RNA was extracted from whole mosquitoes to verify gene knock-down and from dissected heads, abdomens, thoraxes and midguts to perform tissue and infection-responsive expression analyses using Trizol (TRIzol Reagent, Thermo Fisher Scientific) according to the manufacturer's instructions. Quantitative real-time PCR (qRT-PCR) was carried out using SYBR Green Master Mix for qPCR (Thermo Fisher Scientific) on a StepOnePlus Real-Time PCR System with the StepOne Software (Thermo Fisher Scientific) for data analysis. Transcript abundance was normalized to *A. gambiae* ribosomal protein S7 gene levels, and the fold change of each gene was calculated using the $\Delta\Delta Ct$ method (comparative cycle threshold (Ct) method, also known as the $2^{(-\Delta\Delta Ct)}$ method)⁵⁵. The primers for each gene are presented in Supplementary Table 1. The primers were synthesized through Integrated DNA Technologies (IDT).

RNAi-mediated gene silencing and *Plasmodium* infection assays

The function of selected genes was assayed using RNAi-mediated gene silencing as described previously⁵⁶. Specifically, dsRNAs were synthesized from PCR products using the HiScribe T7 in vitro transcription kit (New England Biolabs). The primer sequences are listed in Supplementary Table 1. Approximately 69 nl of dsRNAs ($3 \mu\text{g } \mu\text{l}^{-1}$, 200 ng per mosquito) targeting genes of interest or *Gfp* as a control was injected into the thorax of cold-anaesthetized 4-day-old female mosquitoes using a nano-injector (Drummond Scientific Nanoject II) with a glass capillary. Three days after injection, groups of six mosquitoes were collected for silencing efficiency measurement using qRT-PCR with primers listed in Supplementary Table 1; the KD efficiencies (KD%) are presented in Supplementary Table 1. At least three biological replicates were included for each gene. Three days after dsRNA injection and validation of gene silencing, the mosquitoes were fed on *P. falciparum* NF54 (BEI Resources, MRA-1000 *P. falciparum*, NF54 (Patient Line E)) gametocyte culture (provided by Johns Hopkins Malaria Research Institute Parasitology Core Facility) through artificial glass membrane feeders (Chemglass CG-1836-75) or a wild-type *P. berghei* (ANKA2.33)-infected mouse as described^{23–25,57}. After unfed females were removed, the mosquitoes were kept for 8 days at 27 °C for *P. falciparum* infection and 12 days at 19 °C for *P. berghei* infection before midgut dissection. At least three independent biological replicates were performed for each experiment, with at least 80 mosquitoes in each replicate. Midguts were dissected in PBS and stained in 0.1% mercurochrome (in PBS) for at least 20 min to determine oocyst numbers using a Leica microscope (DM1000 Phase Contrast & Darkfield). Significant differences in the infection intensity between control and

treated groups were determined through the Mann–Whitney *U* test (two tailed). Prevalence is the percentage of mosquitoes with at least one oocyst on their midgut. Fisher's exact test was used to assess the significance of infection prevalence. The dot plots of the oocyst loads within each treatment and a small pie chart above each sample indicating the infection prevalence were produced with GraphPad Prism 10 software, with the median value indicated by the red bars. A detailed statistical analysis of all infection assays done in this study is presented in Supplementary Table 2.

Anti-PFDN6 polyclonal antibody preparation and IgG purification

Recombinant PFDN6 protein was first expressed in insect Sf9 cells (Thermo Fisher Scientific) and *E. coli* as described²⁷. In particular, the gene encoding PFDN subunit 6 (*Pfdn6*) was amplified from *A. gambiae* cDNA by PCR with *Pfx* DNA polymerase (Thermo Fisher Scientific) using specific primers with the restriction sites indicated in Supplementary Table 1. PCR products were subcloned into the pLEX10 and pET28 expression vectors. The clones were transformed into Sf9 insect cells (Thermo Fisher Scientific) for the pLEX10 construct or *E. coli* strain BL21 for the pET28 construct, and the recombinant proteins were produced in these corresponding cells. The recombinant *A. gambiae* proteins were purified by Strep II fusion tag (Sigma) for the pLEX10 construct and Ni-NTA agarose gel (Thermo Fisher Scientific) for the pET28 construct, following the manufacturer's instructions and protocol as described previously²⁷, then concentrated and buffer-exchanged with PBS by using 10-kDa Amicon Ultra Centrifugal Filters (MilliporeSigma). The concentrations of proteins were determined using either a Bradford assay kit (Bio-Rad) or the Micro BCA Protein Assay Kit (Thermo Fisher Scientific) with various concentrations of BSA as standard following the manufacturer's instructions.

About 1 mg of recombinant PFDN6 protein in PBS was sent to Washington Biotechnology to immunize two rabbits and produce antiserum. The total immunoglobulin (IgG) of PFDN6 or control (GFP) antibody was purified using Agarose-A beads (Pierce Protein A Agarose, Thermo Fisher Scientific), following the manufacturer's instructions and published method²⁷.

Assays for antibody-blocking *P. falciparum* and *P. vivax* infection

Antibody-blocking assays were performed using polyclonal anti-PFDN6 or anti-GFP antibodies as a control. Various concentrations of antibodies diluted in PBS (1/10 volume of blood) were added directly to an infectious blood meal containing *P. falciparum* or *P. vivax* before being used to feed 4-day-old female mosquitoes through an artificial glass membrane feeder (Chemglass CG-1836-75). *P. vivax*-infected blood (drawn from gametocyte carriers in Thailand) was used for *P. vivax* infection assays. After unfed females were removed, mosquitoes were incubated and dissected as described above to determine oocyst-stage infection intensity.

Immunization of mice with PFDN6 protein, antibody titration through ELISA and transmission-blocking assay with *P. berghei* parasites

Groups of 5–6-week-old Swiss Webster mice were subcutaneously immunized with 10 µg of rPFDN6 in Imject Freund's Complete Adjuvant (Thermo Fisher Scientific). By contrast, a control group received recombinant GFP protein or PBS in the same volume. Five mice received subcutaneous injections of 10 µg rPFDN6 in Freund's adjuvant at 2-week intervals; 2 weeks later, the same amount of protein with half of the adjuvant was administered to boost the immunization based on published protocol^{34,35}. Controls received recombinant GFP or PBS injections using the same protocol. Four weeks after the final injection, the collected mouse serum showed high-titre antibody concentrations, as determined by ELISA, following the established protocol³⁵. Specifically,

mouse sera collected at 4 weeks after vaccination were used. Purified rPFDN6, after affinity purification using the protocol described above, was diluted to 0.5 µg ml⁻¹ in a binding buffer of 0.1 M sodium phosphate (Na₂HPO₄, pH 9.0) and coated onto a 96-well MediSorp ELISA plate (Nunc) overnight at 4 °C. The plate was then washed three times with PBST (0.2% Tween 20 in PBS, pH 7.4) and blocked with BSA (2.5%) and goat serum (1%) in PBS for 2 h at room temperature. Serum samples were serially diluted from 1:1,000 to 1,024,000 at 1:4 serial dilutions. Alkaline phosphatase-conjugated goat anti-mouse IgG (Sigma-Aldrich) was used for detecting bound IgG, and *p*-nitrophenyl phosphate (Sigma-Aldrich) served as the substrate for visualization using a microplate spectrophotometer (Thermo Fisher Scientific) with absorbance (optical density) measured at 450 nm. Three mice with high titres of PFDN6 antibody were then infected with *P. berghei* parasites via intraperitoneal (IP) injection (Extended Data Fig. 1e,f). Once parasitaemia and gametocytaemia (determined by Giemsa (Sigma) staining) had reached 8% and 2.5%, respectively, at 2–3 days after *P. berghei* infection, *A. gambiae* mosquitoes were infected with *P. berghei* (Pb)-infected mice through direct skin feeding on the PFDN6 or control vaccinated Pb-infected mice. Blood-fed mosquitoes were subsequently incubated under the described conditions before dissection, and oocyst counts were assayed as described above.

Counting of ookinetes and sporozoites

After mosquitoes were fed on infectious blood containing either anti-PFDN6 antibody or anti-GFP antibody as a control, they were incubated under the specified conditions for 24–28 h, followed by dissection of the midguts. Ookinete counting in the mosquito guts and lumen followed the established methodology^{57,58}, with minor modifications. Entire guts, including the blood meal contents, were placed in Corning 96-well plates filled with 30 µl of sterile PBS (in each well) and homogenized individually by repeated pipetting. Subsequently, 10 µl of this homogenate was spotted on Teflon-printed microwell glass slides with a 10-mm-diameter circle (VWR International). The sample slides were air-dried, fixed with methanol and stained with 2×-diluted Giemsa stain (Sigma) for 5 min, then analysed under a Leica microscope (DM1000 Phase Contrast & Darkfield). The number of ookinetes in each spotted sample was counted, and average values for the ookinete densities were calculated from at least three biological replicates with at least 12 midgut samples in each replicate. These average values were then multiplied by the dilution factor of the sample (1 in 3) to estimate the total number of ookinetes present within the entire blood bolus.

The method outlined in a previous study⁵⁹ was used to determine sporozoite loads in the salivary glands of infected mosquitoes. Specifically, salivary glands were dissected, and individual pairs of glands were placed in Eppendorf tubes with 120 µl of PBS. Subsequently, the glands were homogenized on ice manually using plastic pestles (KIMBLE Disposable Pellet Pestle: Polypropylene, 0.5 ml capacity), followed by centrifugation with an Eppendorf 5424 Centrifuge at 9,000 × *g* for 10 min. Approximately 90 µl of the supernatant was then removed. The remaining sporozoites were resuspended in the final 30 µl of PBS, and 10 µl of this suspension was placed in a Neubauer counting chamber. After the homogenate was placed in the counting chamber for 10 min, the sporozoites were counted using a Leica phase-contrast microscope (DM1000 Phase Contrast & Darkfield) at ×400 magnification.

Western blot analysis

Western blot hybridization was done essentially, according to a previous study²⁷, with modifications. Dissected midguts, thoraxes, abdomens, perfused haemolymph (prepared based on published protocols^{60,61}) and different *A. gambiae* immune-competent cell lines²⁷ were prepared and lysed in RIPA buffer (Sigma-Aldrich). The total perfused haemolymph with haemocytes was filtered through a 0.22 µm pore filter (MilliporeSigma Ultrafree Centrifugal Filter, 0.5 ml sample volume, UFC30GV0S) using an Eppendorf centrifuge at a low speed

of $1,000 \times g$ to collect a cell-free haemolymph sample. The cell total protein concentration in the cell lysate supernatant was measured through a Bradford Protein Assay (Bio-Rad). A total of 10 µg protein from a different tissue or cell line lysate was mixed with NuPAGE LDS Sample Buffer (Thermo Fisher Scientific), heated at 95 °C for 10 min and separated on a Novex Tris-Glycine Mini Protein Gels (4–20% gradient, 1.0 mm, WedgeWell, Thermo Fisher Scientific). Proteins were transferred to nitrocellulose membranes (Bio-Rad) and incubated in a blocking buffer (PBST (1× PBS with 0.1% Tween 20), 5% w/v nonfat dry milk) for 1 h. Blots were incubated for 1 h in primary antibody diluted in PBST, washed three times with PBST and then incubated for 1 h in secondary antibody diluted in PBST. Membranes were washed three times with PBST, and blots were developed using ECL Prime western blotting detection reagent (Cytiva Amersham). All incubations were performed at room temperature. As described above, a rabbit polyclonal anti-PFDN6 antibody (Washington Biotechnology) was produced using recombinant PFDN6 protein. The total protein concentrations were measured through Bradford (Bio-Rad) assay or using a Micro BCA Protein kit (Thermo Fisher Scientific) to load the same amount of total proteins (10 µg per sample) as a loading control for western blot analysis. Serially diluted BSA was used to establish a working curve and determine the total protein concentration in the samples. Mouse β-actin monoclonal antibody (Abcam, mAbcam 82260) was used as a second loading control with a final dilution of 1:5,000. Anti-rabbit and anti-mouse secondary antibodies conjugated to horseradish (HRP) (Abcam) were used at a final dilution of 1:15,000.

Immunofluorescence assay and confocal microscopy

As previously described^{50,58}, immunostaining for confocal microscopy was performed by using mouse anti-Pfs25 (BEI resources, catalogue number MRA-28), rabbit anti-laminin polyclonal antibody (Thermo Fisher Scientific, catalogue number PA5-115490), rabbit anti-Tep1 polyclonal antibody (previously generated⁵⁰ from Boster Bio) and rabbit anti-PFDN6 primary antibodies at a 1:500 dilution. The secondary antibodies were obtained from Thermo Fisher Scientific with AlexaFluor 488-conjugated (green) goat anti-mouse or AlexaFluor 568-conjugated (red) goat anti-mouse antibody (1:500 dilution) for the parasite-specific antibodies (anti-Pfs25). AlexaFluor 568-conjugated (red) goat anti-rabbit antibody (1:500 dilution) was used for anti-Tep1, anti-laminin and anti-PFDN6 antibodies. The filament actin was stained with Alexa-488-conjugated phalloidin (Thermo Fisher Scientific). The samples were examined with a Zeiss LSM 700 confocal microscope (at Johns Hopkins School of Medicine Microscope Facility), collecting 0.2 mm to 1 mm optical sections with Z-stacks. The images were analysed, and the projections of the Z-stack images were prepared through Zeiss Zen lite (Zeiss). For the comparison across different slides, the confocal microscopy settings were kept at the same levels, and DAPI (Thermo Fisher Scientific) staining of the nuclei from each treatment was used for standardization. The fluorescent intensities from the co-localization of total Tep1, laminin protein with *P.falciparum* ookinetes or oocysts were measured with the ImageJ (Fiji) software. A total of 20 midguts (with at least 3 parasites in each gut) were assayed for each treatment. The intensities of the green fluorescence of *P.falciparum* oocyst samples were used as internal references for normalization. The absolute intensities of 20 representative ookinetes or oocysts (green) and Tep1- (red) or laminin-protein (red) are presented in Supplementary Tables 4–6.

Co-IP assay to identify PFDN6 interaction proteins

Co-IP assay for identifying the PFDN6 interacting proteins was done based on established protocol^{44,62–64} with modifications. About 100 female mosquitoes were anaesthetized with ice and injected with 69 nl of recombinant PFDN6 protein (2.5 µg µl⁻¹ in PBS) or controls with PBS alone using a Nanoject II Injector (Drummond). After injection, the mosquitoes were left in a container for 3 h. Then, they were collected

on ice in 1 ml IP buffer (Tris-HCl 50 mM (pH 7.9), NaCl 100 mM, EDTA 2 mM, BSA 0.1 µg ml⁻¹, Tween 20 0.1% w/v) and homogenized thoroughly afterwards. Lipids and debris were removed by a couple of rounds of centrifugation using an Eppendorf centrifuge at 9,000 × g. Samples were kept at 4 °C under constant shaking. For pre-clearance, extracts were incubated for 1 h with 30 µl of Protein A-Sepharose bead slurry (GE Healthcare). The supernatant was next incubated for 1 h with 1 µg PFDN6 polyclonal antibody and subsequently with 30 µl of Protein A-Sepharose for another hour. Samples were centrifuged, and post-IP supernatant was collected. Sepharose beads were washed at least four times by using alternating wash buffer 1 (Tris-HCl 50 mM (pH 7.9), Tween 20 0.1% w/v) and wash buffer 2 (buffer 1 plus NaCl 500 mM). Antibodies and bound proteins were eluted from the beads in 40 µl protein loading buffer at 95 °C for 3 min. Aliquots of post-IP supernatant and eluates were separated by Novex 4–20% Tris-Glycine gradient sodium dodecyl sulfate-polyacrylamide gel electrophoresis (Thermo Fisher Scientific). The gel was fixed and stained with a Colloidal Blue Staining Kit (Thermo Fisher Scientific, LC6025). The samples from the PBS-injected group were used as a loading control, and the specific protein bands identified in cohorts injected with rPFDN6 were excised from the gel for mass spectrometry sequencing as described in previous publications^{65,66}.

Mosquito midgut microbiota enumeration, antibiotic treatment and mortality assays

Bacterial colony forming unit (CFU) assays, 16S rRNA expression to determine the bacterial loads from the mosquito midgut and antibiotic treatment to remove the mosquito microbiota were done essentially according to established protocols^{23,67}. The midguts from surface-sterilized mosquitoes were dissected with sterilized PBS 4 days after treatments, and CFU was determined by plating the midgut homogenate with serial dilutions on Luria-Bertani agar plates and incubating the plates at 27 °C for 2 days. Each assay had at least nine independent midguts in each replicate, and three biological replicates were included. The mosquitoes were treated with antibiotics to remove natural microbiota. After emergence, adult female mosquitoes were daily given fresh filtered sterilized 10% sucrose solution containing 15 µg ml⁻¹ gentamicin sulfate (Sigma) and 10 units ml⁻¹ penicillin and 10 µg ml⁻¹ streptomycin (Invitrogen). The mosquito mortality and related assays were done according to previously published protocols⁵⁷. To measure the survival of the mosquitoes after treatments, treated mosquitoes were placed into cups with a cotton pad constantly impregnated with a 10% sucrose solution. They were held in the cups 8 days after treatment, the number of dead mosquitoes in the cup was recorded and the dead mosquitoes were removed daily. The survival percentage represents the mean survival percentage for all three biological replicates of 35 mosquitoes each. Statistical significance was determined by Kaplan-Meier survival analysis with pooled data from three replicates using GraphPad Prism10 software, and Pvalues were determined by Wilcoxon test. The phagocytic index was determined according to previously published protocols⁶⁸. The mosquito haemolymph was perfused 24 h after oral ingestion of FITC-labelled *E. coli*, and the number of haemocytes with or without green fluorescence was counted under a Leica fluorescence microscope with $\times 1,000$ magnification. The phagocytic index was determined using the following equation: phagocytic index = (number of particles internalized × number of phagocytosing cells)/total number of cells analysed. At least 20 fields were examined for each sample and at least 7 replicates were included for each treatment.

Generation of CRISPR-Cas9-mediated *Pfdn6* knockout mutants

To generate CRISPR-Cas9-mediated *Pfdn6* gene knockout mutants, we first generated guide RNA (gRNA)-expressing transgenics, as previously published⁶⁹. Two web tools, <http://crispr.mit.edu> and CHOP-CHOP, were applied to design gRNA sequences, and potential off-target

binding sites were checked through CHOPCHOP (<https://chopchop.cbu.uib.no/>). We selected three gRNA targets, and the forward and reverse primers (for linker sequences) were synthesized through IDT. Linker sequences were individually cloned into three pBluescript-based cloning vectors for cloning synthetic gRNA sequences (pSKB-sgRNAs) and assembled into pDSAR (docking site transgenesis plasmid for GoldenGate cloning and insect transgenesis), followed by embryo microinjection of the *A. gambiae* docking line X1 (ref. 70). Approximately 500 embryos were injected for the construct, with a 14% hatching rate and 28% of surviving larvae showing transient positive expression of the eye-specific fluorescent markers (red fluorescence for *Pfdn6*-gRNA). The fourth generation (G4) gRNA-expressing lines were crossed with the germ-line-expressing Cas9 strain (Vasa::Cas9; with green and yellow fluorescence in the eyes) to establish *Pfdn6* somatic knockout mutants by screening the positive *Pfdn6*-gRNA/Cas9 transheterozygotes with both red and green fluorescence in the eyes. The mutation region was amplified by leg PCR as described before using a Phire kit (Thermo Fisher Scientific, dilution protocol for one leg) with flanking primers listed in Supplementary Table 1, followed by Sanger sequencing (performed at Poochoon Scientific) to confirm the mutation.

Statistics and reproducibility

All statistical analyses were performed using GraphPad Prism 10.0 for Windows (GraphPad), using unpaired Student's *t*-test (two tailed) for parametric analysis or the Mann–Whitney *U* test (two tailed) for non-parametric analysis of infection intensities. The infection prevalence was determined through Fisher's exact test. One-way ANOVA was used to determine the significance of gene expression at various time points. Mean values are presented alongside standard error (s.e.) bars. Kaplan–Meier survival analysis was used to determine the significance of survival probabilities. Significance was assessed at **P*<0.05, ***P*<0.01, ****P*<0.001 and *****P*<0.0001. Exact *P* values for infection prevalences and intensities were presented and are provided either in the figure itself or in Supplementary Table 2, along with detailed information. The exact *P* values are included in the source data for gene expression.

Reporting summary

Further information on research design is available in the Nature Portfolio Reporting Summary linked to this article.

Data availability

All data generated or analysed in this study are included in the article and Supplementary Information. Additional information is available from the corresponding author upon request. Source data are provided with this paper.

References

- Simoes, M. L., Caragata, E. P. & Dimopoulos, G. Diverse host and restriction factors regulate mosquito–pathogen interactions. *Trends Parasitol.* **34**, 603–616 (2018).
- Dong, S., Dong, Y., Simoes, M. L. & Dimopoulos, G. Mosquito transgenesis for malaria control. *Trends Parasitol.* **38**, 54–66 (2022).
- Gestaut, D. et al. The chaperonin TRiC/CCT associates with prefoldin through a conserved electrostatic interface essential for cellular proteostasis. *Cell* **177**, 751–765.e15 (2019).
- Gestaut, D., Limatola, A., Joachimiak, L. & Frydman, J. The ATP-powered gymnastics of TRiC/CCT: an asymmetric protein folding machine with a symmetric origin story. *Curr. Opin. Struct. Biol.* **55**, 50–58 (2019).
- Vlachou, D., Schlegelmilch, T., Christophides, G. K. & Kafatos, F. C. Functional genomic analysis of midgut epithelial responses in *Anopheles* during *Plasmodium* invasion. *Curr. Biol.* **15**, 1185–1195 (2005).
- Mendes, A. M. et al. Conserved mosquito/parasite interactions affect development of *Plasmodium falciparum* in Africa. *PLoS Pathog.* **4**, e1000069 (2008).
- Liang, J. et al. The functions and mechanisms of prefoldin complex and prefoldin-subunits. *Cell Biosci.* **10**, 87 (2020).
- Herranz-Montoya, I., Park, S. & Djouder, N. A comprehensive analysis of prefoldins and their implication in cancer. *iScience* **24**, 103273 (2021).
- Arranz, R., Martin-Benito, J. & Valpuesta, J. M. Structure and function of the cochaperone prefoldin. *Adv. Exp. Med. Biol.* **1106**, 119–131 (2018).
- Hansen, W. J., Cowan, N. J. & Welch, W. J. Prefoldin-nascent chain complexes in the folding of cytoskeletal proteins. *J. Cell Biol.* **145**, 265–277 (1999).
- Putra, V. D. L., Kilian, K. A. & Knothe Tate, M. L. Biomechanical, biophysical and biochemical modulators of cytoskeletal remodeling and emergent stem cell lineage commitment. *Commun. Biol.* **6**, 75 (2023).
- Tahmaz, I., Shahmoradi Ghahe, S. & Topf, U. Prefoldin function in cellular protein homeostasis and human diseases. *Front. Cell Dev. Biol.* **9**, 816214 (2021).
- Blandin, S. et al. Complement-like protein TEP1 is a determinant of vectorial capacity in the malaria vector *Anopheles gambiae*. *Cell* **116**, 661–670 (2004).
- Christophides, G. K. et al. Immunity-related genes and gene families in *Anopheles gambiae*. *Science* **298**, 159–165 (2002).
- Volohonsky, G. et al. Kinetics of *Plasmodium* midgut invasion in *Anopheles* mosquitoes. *PLoS Pathog.* **16**, e1008739 (2020).
- Smith, R. C. & Barillas-Mury, C. *Plasmodium* oocysts: overlooked targets of mosquito immunity. *Trends Parasitol.* **32**, 979–990 (2016).
- Clayton, A. M., Dong, Y. & Dimopoulos, G. The *Anopheles* innate immune system in the defense against malaria infection. *J. Innate Immun.* **6**, 169–181 (2014).
- Shiao, S. H., Whitten, M. M., Zachary, D., Hoffmann, J. A. & Levashina, E. A. Fz2 and cdc42 mediate melanization and actin polymerization but are dispensable for *Plasmodium* killing in the mosquito midgut. *PLoS Pathog.* **2**, e133 (2006).
- Maya-Maldonado, K. et al. *Plasmodium* exposure alters midgut epithelial cell dynamics during the immune memory in *Anopheles albimanus*. *Dev. Comp. Immunol.* **133**, 104424 (2022).
- Keleta, Y., Ramelow, J., Cui, L. & Li, J. Molecular interactions between parasite and mosquito during midgut invasion as targets to block malaria transmission. *NPJ Vaccines* **6**, 140 (2021).
- Castillo, J. C., Ferreira, A. B. B., Trisnadi, N. & Barillas-Mury, C. Activation of mosquito complement antiplasmoidal response requires cellular immunity. *Sci. Immunol.* **2**, eaal1505 (2017).
- Rodgers, F. H., Gendrin, M., Wyer, C. A. S. & Christophides, G. K. Microbiota-induced peritrophic matrix regulates midgut homeostasis and prevents systemic infection of malaria vector mosquitoes. *PLoS Pathog.* **13**, e1006391 (2017).
- Dong, Y., Manfredini, F. & Dimopoulos, G. Implication of the mosquito midgut microbiota in the defense against malaria parasites. *PLoS Pathog.* **5**, e1000423 (2009).
- Dong, Y. et al. *Anopheles gambiae* immune responses to human and rodent *Plasmodium* parasite species. *PLoS Pathog.* **2**, e52 (2006).
- Garver, L. S., Dong, Y. & Dimopoulos, G. Caspar controls resistance to *Plasmodium falciparum* in diverse anopheline species. *PLoS Pathog.* **5**, e1000335 (2009).
- Gupta, L., Kumar, S., Han, Y. S., Pimenta, P. F. & Barillas-Mury, C. Midgut epithelial responses of different mosquito–*Plasmodium* combinations: the actin cone zipper repair mechanism in *Aedes aegypti*. *Proc. Natl Acad. Sci. USA* **102**, 4010–4015 (2005).

27. Sandiford, S. L. et al. Cytoplasmic actin is an extracellular insect immune factor which is secreted upon immune challenge and mediates phagocytosis and direct killing of bacteria, and is a *Plasmodium* antagonist. *PLoS Pathog.* **11**, e1004631 (2015).
28. Melville, M. W., McClellan, A. J., Meyer, A. S., Darveau, A. & Frydman, J. The Hsp70 and TRiC/CCT chaperone systems cooperate in vivo to assemble the Von Hippel–Lindau tumor suppressor complex. *Mol. Cell. Biol.* **23**, 3141–3151 (2003).
29. Vaughan, J. A., Noden, B. H. & Beier, J. C. Sporogonic development of cultured *Plasmodium falciparum* in six species of laboratory-reared *Anopheles* mosquitoes. *Am. J. Trop. Med. Hyg.* **51**, 233–243 (1994).
30. Belachew, E. B. Immune response and evasion mechanisms of *Plasmodium falciparum* parasites. *J. Immunol. Res.* **2018**, 6529681 (2018).
31. Healy, S. A. et al. Pfs230 yields higher malaria transmission-blocking vaccine activity than Pfs25 in humans but not mice. *J. Clin. Invest.* **131**, e146221 (2021).
32. Dinglasan, R. R. et al. *Plasmodium falciparum* ookinete require mosquito midgut chondroitin sulfate proteoglycans for cell invasion. *Proc. Natl Acad. Sci. USA* **104**, 15882–15887 (2007).
33. Zhang, G. et al. *Anopheles* midgut FREP1 mediates *Plasmodium* invasion. *J. Biol. Chem.* **290**, 16490–16501 (2015).
34. Schleicher, T. R. et al. A mosquito salivary gland protein partially inhibits *Plasmodium* sporozoite cell traversal and transmission. *Nat. Commun.* **9**, 2908 (2018).
35. Niu, G. et al. The fibrinogen-like domain of FREP1 protein is a broad-spectrum malaria transmission-blocking vaccine antigen. *J. Biol. Chem.* **292**, 11960–11969 (2017).
36. Dogterom, M. & Koenderink, G. H. Actin–microtubule crosstalk in cell biology. *Nat. Rev. Mol. Cell Biol.* **20**, 38–54 (2019).
37. Preciado Lopez, M. et al. Actin–microtubule coordination at growing microtubule ends. *Nat. Commun.* **5**, 4778 (2014).
38. Johnson, R. M., Cozens, D. W., Ferdous, Z., Armstrong, P. M. & Brackney, D. E. Increased blood meal size and feeding frequency compromise *Aedes aegypti* midgut integrity and enhance dengue virus dissemination. *PLoS Negl. Trop. Dis.* **17**, e0011703 (2023).
39. Kwon, H., Simoes, M. L., Reynolds, R. A., Dimopoulos, G. & Smith, R. C. Additional feeding reveals differences in immune recognition and growth of *Plasmodium* parasites in the mosquito host. *mSphere* **6**, e00136-21 (2021).
40. Dong, S. et al. Chikungunya virus dissemination from the midgut of *Aedes aegypti* is associated with temporal basal lamina degradation during bloodmeal digestion. *PLoS Negl. Trop. Dis.* **11**, e0005976 (2017).
41. Djihinto, O. Y. et al. Malaria-transmitting vectors microbiota: overview and interactions with *Anopheles* mosquito biology. *Front. Microbiol.* **13**, 891573 (2022).
42. Dong, Y. & Dimopoulos, G. *Anopheles* fibrinogen-related proteins provide expanded pattern recognition capacity against bacteria and malaria parasites. *J. Biol. Chem.* **284**, 9835–9844 (2009).
43. Kobe, B. & Deisenhofer, J. The leucine-rich repeat: a versatile binding motif. *Trends Biochem. Sci.* **19**, 415–421 (1994).
44. Povelones, M., Waterhouse, R. M., Kafatos, F. C. & Christophides, G. K. Leucine-rich repeat protein complex activates mosquito complement in defense against *Plasmodium* parasites. *Science* **324**, 258–261 (2009).
45. Arrighi, R. B. G. & Hurd, H. The role of *Plasmodium berghei* ookinete proteins in binding to basal lamina components and transformation into oocysts. *Int. J. Parasitol.* **32**, 91–98 (2002).
46. Nacer, A., Walker, K. & Hurd, H. Localisation of laminin within *Plasmodium berghei* oocysts and the midgut epithelial cells of *Anopheles stephensi*. *Parasit. Vectors* **1**, 33 (2008).
47. Vlachou, D. et al. Real-time, in vivo analysis of malaria ookinete locomotion and mosquito midgut invasion. *Cell. Microbiol.* **6**, 671–685 (2004).
48. Mahairaki, V., Voyatzis, T., Siden-Kiamos, I. & Louis, C. The *Anopheles gambiae* gamma1 laminin directly binds the *Plasmodium berghei* circumsporozoite- and TRAP-related protein (CTRP). *Mol. Biochem. Parasitol.* **140**, 119–121 (2005).
49. Vlachou, D. et al. *Anopheles gambiae* laminin interacts with the P25 surface protein of *Plasmodium berghei* ookinete. *Mol. Biochem. Parasitol.* **112**, 229–237 (2001).
50. Simoes, M. L., Dong, Y., Mlambo, G. & Dimopoulos, G. C-type lectin 4 regulates broad-spectrum melanization-based refractoriness to malaria parasites. *PLoS Biol.* **20**, e3001515 (2022).
51. Ferdous, Z. et al. *Anopheles coluzzii* stearoyl-CoA desaturase is essential for adult female survival and reproduction upon blood feeding. *PLoS Pathog.* **17**, e1009486 (2021).
52. Gantz, V. M. et al. Highly efficient Cas9-mediated gene drive for population modification of the malaria vector mosquito *Anopheles stephensi*. *Proc. Natl Acad. Sci. USA* **112**, E6736–E6743 (2015).
53. Hammond, A. et al. A CRISPR-Cas9 gene drive system targeting female reproduction in the malaria mosquito vector *Anopheles gambiae*. *Nat. Biotechnol.* **34**, 78–83 (2016).
54. Carballar-Lejarazu, R. et al. Dual effector population modification gene-drive strains of the African malaria mosquitoes, *Anopheles gambiae* and *Anopheles coluzzii*. *Proc. Natl Acad. Sci. USA* **120**, e2221118120 (2023).
55. Pfaffl, M. W. A new mathematical model for relative quantification in real-time RT-PCR. *Nucleic Acids Res.* **29**, e45 (2001).
56. Garver, L. & Dimopoulos, G. Protocol for RNAi assays in adult mosquitoes (*A. gambiae*). *J. Vis. Exp.* **5**, 230 (2007).
57. Dong, Y. et al. Engineered *Anopheles* immunity to *Plasmodium* infection. *PLoS Pathog.* **7**, e1002458 (2011).
58. Dong, Y., Cirimotich, C. M., Pike, A., Chandra, R. & Dimopoulos, G. *Anopheles* NF-κB-regulated splicing factors direct pathogen-specific repertoires of the hypervariable pattern recognition receptor AgDscam. *Cell Host Microbe* **12**, 521–530 (2012).
59. Dong, Y., Simoes, M. L. & Dimopoulos, G. Versatile transgenic multistage effector-gene combinations for *Plasmodium falciparum* suppression in *Anopheles*. *Sci. Adv.* **6**, eaay5898 (2020).
60. Rodrigues, J., Brayner, F. A., Alves, L. C., Dixit, R. & Barillas-Mury, C. Hemocyte differentiation mediates innate immune memory in *Anopheles gambiae* mosquitoes. *Science* **329**, 1353–1355 (2010).
61. Smith, R. C., Barillas-Mury, C. & Jacobs-Lorena, M. Hemocyte differentiation mediates the mosquito late-phase immune response against *Plasmodium* in *Anopheles gambiae*. *Proc. Natl Acad. Sci. USA* **112**, E3412–E3420 (2015).
62. Baxter, R. H. et al. A heterodimeric complex of the LRR proteins LRIM1 and APL1C regulates complement-like immunity in *Anopheles gambiae*. *Proc. Natl Acad. Sci. USA* **107**, 16817–16822 (2010).
63. Povelones, M. et al. The CLIP-domain serine protease homolog SPCLIP1 regulates complement recruitment to microbial surfaces in the malaria mosquito *Anopheles gambiae*. *PLoS Pathog.* **9**, e1003623 (2013).
64. Kamareddine, L., Nakhleh, J. & Osta, M. A. Functional interaction between apolipoporphins and complement regulate the mosquito immune response to systemic infections. *J. Innate Immun.* **8**, 314–326 (2016).

65. Pike, A., Vadlamani, A., Sandiford, S. L., Gacita, A. & Dimopoulos, G. Characterization of the Rel2-regulated transcriptome and proteome of *Anopheles stephensi* identifies new anti-*Plasmodium* factors. *Insect Biochem. Mol. Biol.* **52**, 82–93 (2014).
66. Saraiva, R. G. et al. Aminopeptidase secreted by *Chromobacterium* sp. Panama inhibits dengue virus infection by degrading the E protein. *PLoS Negl. Trop. Dis.* **12**, e0006443 (2018).
67. Pike, A. et al. Changes in the microbiota cause genetically modified *Anopheles* to spread in a population. *Science* **357**, 1396–1399 (2017).
68. Dong, Y., Taylor, H. E. & Dimopoulos, G. AgDscam, a hypervariable immunoglobulin domain-containing receptor of the *Anopheles gambiae* innate immune system. *PLoS Biol.* **4**, e229 (2006).
69. Dong, Y., Simoes, M. L., Marois, E. & Dimopoulos, G. CRISPR/Cas9-mediated gene knockout of *Anopheles gambiae* FREP1 suppresses malaria parasite infection. *PLoS Pathog.* **14**, e1006898 (2018).
70. Volohonsky, G. et al. Tools for *Anopheles gambiae* transgenesis. *G3* **5**, 1151–1163 (2015).

Acknowledgements

We extend our gratitude to E. Marois (Université de Strasbourg, CNRS UPR9022, INSERM U1257, Institut de Biologie Moléculaire et Cellulaire, Strasbourg, France) for providing the *A. gambiae* X1 and Cas9 lines. We also appreciate the editorial assistance provided by D. McClellan (retired from the Johns Hopkins Welch Medical Library as the director of the Editing Referral Service) and the fruitful discussions with M. Jacobs-Lorena (Johns Hopkins School of Public Health, Malaria Research Institute, United States) and A. Molina-Cruz (Mosquito Immunity and Vector Competence Section, NIAID, NIH, United States). We thank M. Jacobs-Lorena for providing animal protocols for mouse immunization. We acknowledge the Johns Hopkins Malaria Research Institute Parasitology Core Facility, and the Johns Hopkins Institute for Basic Biomedical Sciences Microscope Facility for their support. This study was supported by the National Institutes of Health NIAID grants R01AI158615, R21AI168873, RO1AI170692, R21AI131574 and R01AI122743, the Howard Hughes Medical Institutes grant 90101319, the Bloomberg Philanthropies and the University of California Malaria Initiative. The Walter Reed Army Institute of Research has reviewed the material. There is no objection to its presentation and/or publication. The opinions or assertions contained herein are the private views of

the authors. They are not to be construed as official or as reflecting the actual opinions of the Department of the Army or the Department of Defense. The investigators have adhered to the policies for protecting human subjects as prescribed in AR 70–25.

Author contributions

Conceptualization: Y.D., S.L.S. and G.D. Methodology: Y.D., S.K., S.L.S., A.P., R.U., K.K. and G.D. Investigation and data analysis: Y.D., S.K., S.L.S., A.P., M.L.S., R.U. and K.K. Visualization: Y.D. and G.D. Writing—original draft: Y.D. and G.D. Review and editing: all authors.

Competing interests

The authors declare no competing interests.

Additional information

Extended data is available for this paper at <https://doi.org/10.1038/s41564-025-01947-3>.

Supplementary information The online version contains supplementary material available at <https://doi.org/10.1038/s41564-025-01947-3>.

Correspondence and requests for materials should be addressed to George Dimopoulos.

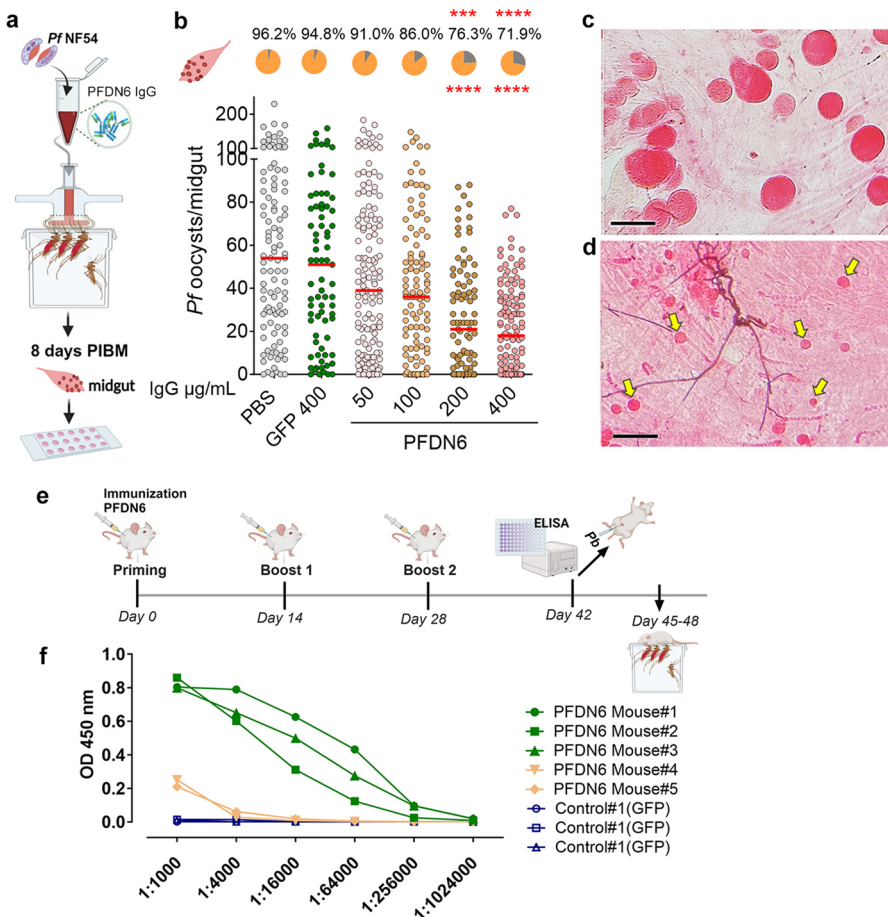
Peer review information *Nature Microbiology* thanks the anonymous reviewers for their contribution to the peer review of this work.

Reprints and permissions information is available at www.nature.com/reprints.

Publisher's note Springer Nature remains neutral with regard to jurisdictional claims in published maps and institutional affiliations.

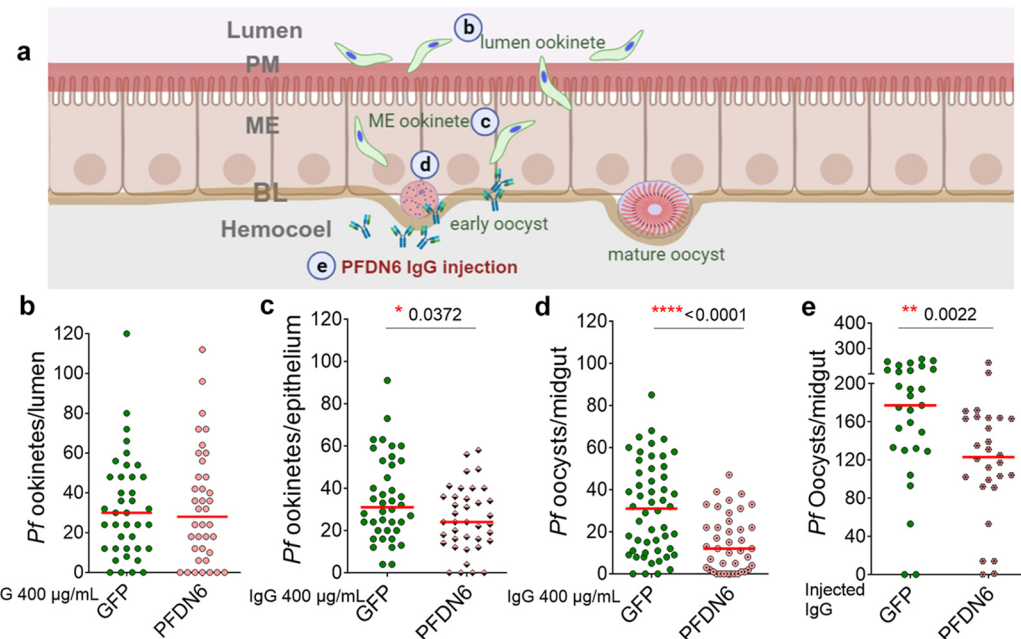
Springer Nature or its licensor (e.g. a society or other partner) holds exclusive rights to this article under a publishing agreement with the author(s) or other rightsholder(s); author self-archiving of the accepted manuscript version of this article is solely governed by the terms of such publishing agreement and applicable law.

© The Author(s), under exclusive licence to Springer Nature Limited 2025



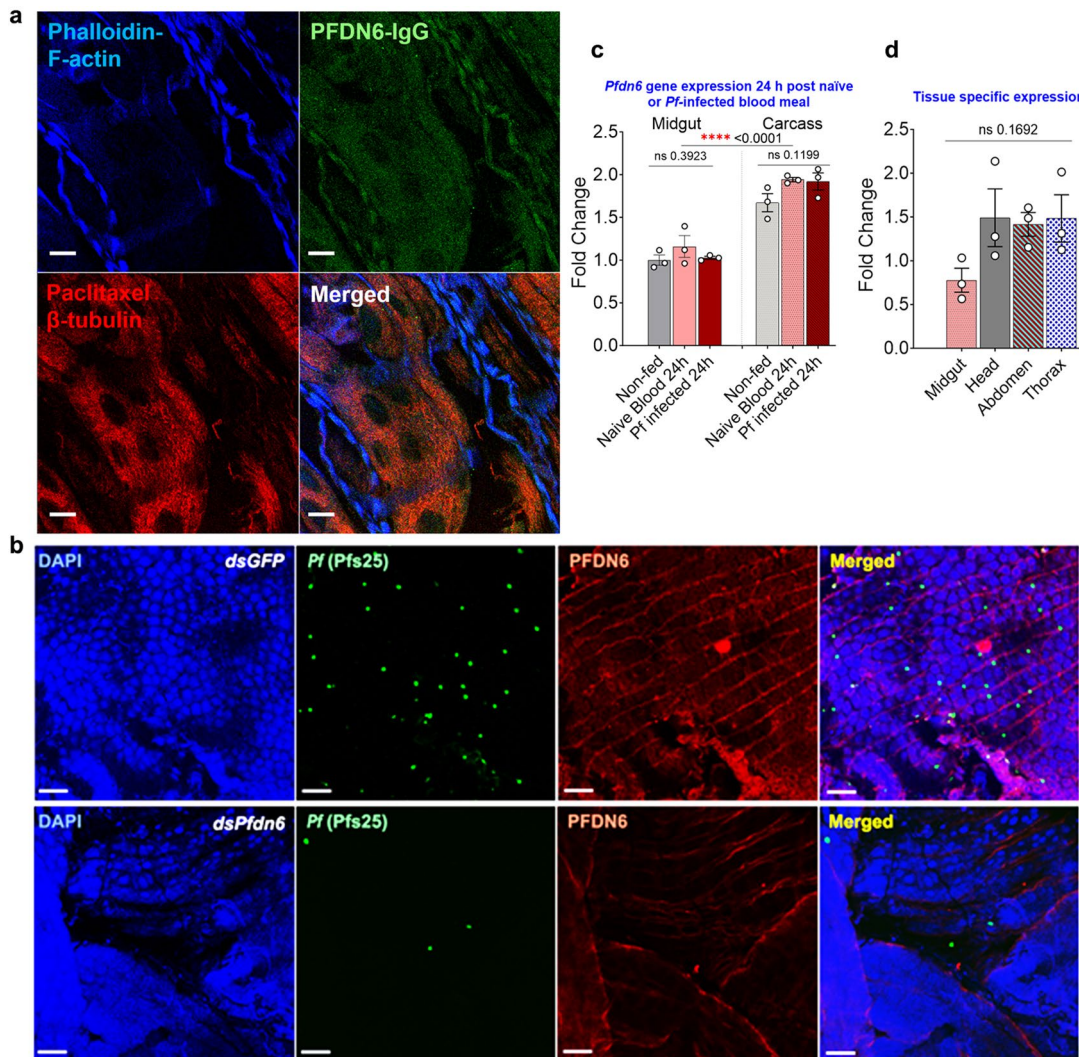
Extended Data Fig. 1 | The blocking effect of anti-PFDN6 antibody on *P. falciparum* parasites in *A. gambiae* mosquito vectors remains effective even at high infection levels and active immunization of mice with PFDN6 recombinant protein (rPFDN6) and titration of PFDN6-specific antibodies by ELISA using rPFDN6 as the antigen. a, An illustration depicting the co-feeding of *P. falciparum* gametocytes with anti-PFDN6 antibodies (PFDN6-IgG) followed by SMFA assays. **b**, Co-feeding of anti-PFDN6 antibody (ranging from 50- to 400- μ g/mL) and *P. falciparum* NF54 gametocytes (0.1% gametocytaria) resulted in significant reductions in the number of oocysts at 8 dpi in *A. gambiae*. Mosquitoes fed with PBS or GFP antibody served as control. Each data point represents the oocyst count in an individual mosquito, with a red line indicating the median number. Small pie charts depict infection prevalence. At least three replicates were conducted, and statistical significance was determined using the Mann-Whitney U test (two-tailed) for infection intensity and Fisher's exact test for infection prevalence. *** $P < 0.001$, **** $P < 0.0001$. Detailed statistical

analysis is included in Supplementary Table 2. **c,d**, Co-feeding mosquitoes with anti-PFDN6 antibody and *P. falciparum* gametocyte-infected blood meals result in smaller oocysts (**d**, yellow arrows) compared to the larger mature oocysts observed in the control co-fed with anti-GFP antibody (**c**) at 8 dpi. Representative microscope images from mercurochrome staining of midguts are shown here. Scale bars, 75 μ m; n = 20. **e**, Schematic overview of the experimental design: Swiss-Webster mice were injected with 50 μ g of recombinant PFDN6 (rPFDN6) or control protein (GFP) and were subsequently boosted twice at two-week intervals. **f**, Two weeks after the final boost, mice were bled and the resulting serum was serially diluted and subjected to antibody titration by ELISA using rPFDN6 as the antigen. Of the five mice initially immunized with rPFDN6, three with high antibody titers were further challenged with *P. berghei*-infected blood. After validating parasitemia and exflagellation, these six mice, including PFDN6 and control GFP immunized mice, were subsequently blood-fed to six cohorts of *A. gambiae* mosquitoes. Figure created with BioRender.com.



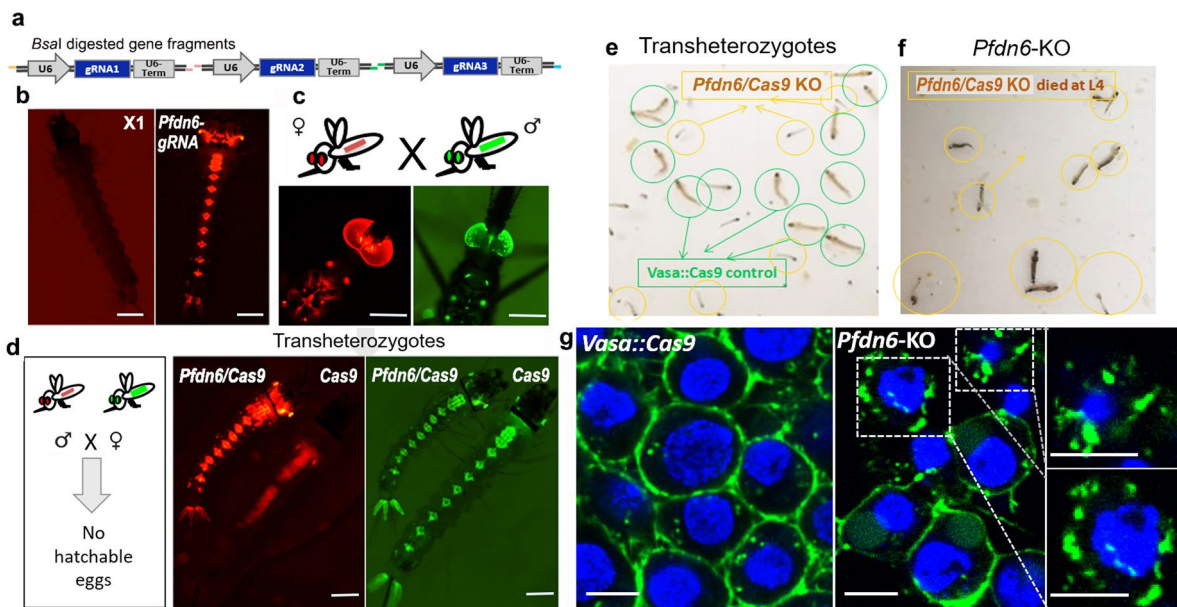
Extended Data Fig. 2 | Elucidating the working mechanisms of when PFDN6 administers its host factor function through co-feeding with anti-PFDN6 antibodies at the final concentration of 400 µg/mL. **a**, An overview illustration of the lumen ookinetes and midgut epithelium ookinetes and the early oocyst resides within the gut basal lamina and delivery of PFDN6 antibodies into the hemolymph through thoracic injection. **b**, No difference in lumen ookinetes numbers was observed comparing the PFDN6-IgG fed group with the ones fed with GFP control antibodies. **c,d**, Significant reduction of epithelium ookinetes (**c**) and early oocysts (**d**) suggesting the Prefoldin complex (PFDN) administers its agonist functions during ookinetes invasion of midgut epithelial. **e**, supplementation of anti-PFDN6 antibodies (PFDN6-IgG) in the hemolymph

through thoracic injection resulted in a significant reduction in oocyst numbers (** $P < 0.01$), suggesting that the blocking activity of the antibodies may be exerted on the basal region of the midgut epithelium. Each data point represents the number of ookinetes or oocysts in an individual mosquito midgut, and the red line indicates the median number. Data were obtained from at least three independent replicates, except for panel (e), which was performed with two replicates. Statistical significance for infection intensity was assessed using the Mann-Whitney test. Note that the infection assays in panels (b) through (d) were not always performed pairwise. * $P < 0.05$, ** $P < 0.01$, **** $P < 0.0001$. Detailed statistical analysis and numbers are included in Supplementary Table 2. Figure created with BioRender.com.



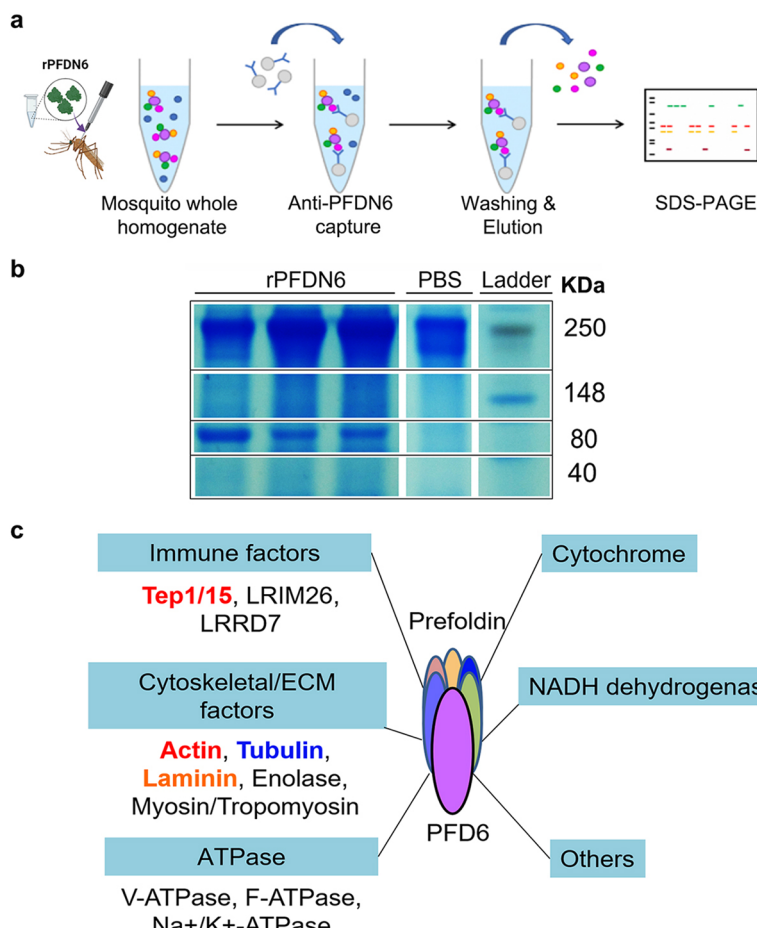
Extended Data Fig. 3 | PFDN6 did not co-localize with parasites, namely ookinetes at 24 h or oocysts at 36 h post-*P. falciparum* infectious blood meal within the midgut epithelial cells, and qRT-PCR expression analysis of *Pfdn6* gene in mosquito tissues. The distribution of PFDN6 is predominantly overlapped with actin and tubulin, along with PFDN6 antibody (PFDN6-IgG) staining of the prefoldin complex, largely overlapped, suggesting the conserved role of PFDN in actin and tubulin polymerization. n = 20; Scale bars: 50 μ m. **b**, PFDN6 exhibited no colocalization with *P. falciparum* ookinetes or early oocysts, indicating that the PFDN complex does not directly interact with *Plasmodium* parasites. However, in the depletion of PFDN6 (*dsPfdn6*), fewer oocysts (in green) developed compared to the control group treated with GFP dsRNA (*dsGFP*). One representative midgut sample is shown here from a total of 10 midguts assayed with at least three parasites in each midgut. DAPI: nuclei in blue; Pfs25: anti-Pfs25 antibodies stain *P. falciparum*

ookinetes and oocysts in green; PFDN6: anti-PFDN6 antibodies stain PFDN complex in red (Alex-568); Merged: three channels were merged. Scale bars, 50 μ m. **c**, qRT-PCR analysis indicates no significant upregulation of *Pfdn6* in either the midguts or carcasses following either a naïve or *P. falciparum* infectious blood meal (*Pf*-infected) 24 h post-feeding, but a significant upregulation in the carcass tissue was identified through one-way ANOVA analysis (****P < 0.0001). **d**, An insignificant trend of higher expression levels of *pfdn6* in the head, abdomen, and thorax tissues. n = 3, with at least ten mosquitoes included per treatment to extract total RNA. Fold changes were calculated using a housekeeping ribosomal S7 gene as an internal control for normalization, with gene-specific details and primer information provided in Supplementary Table 1. Mean values and standard error bars were included to assess the significance of gene expression. Student's t-test (two-tailed) and one-way ANOVA were employed to calculate p-values and determine significance.



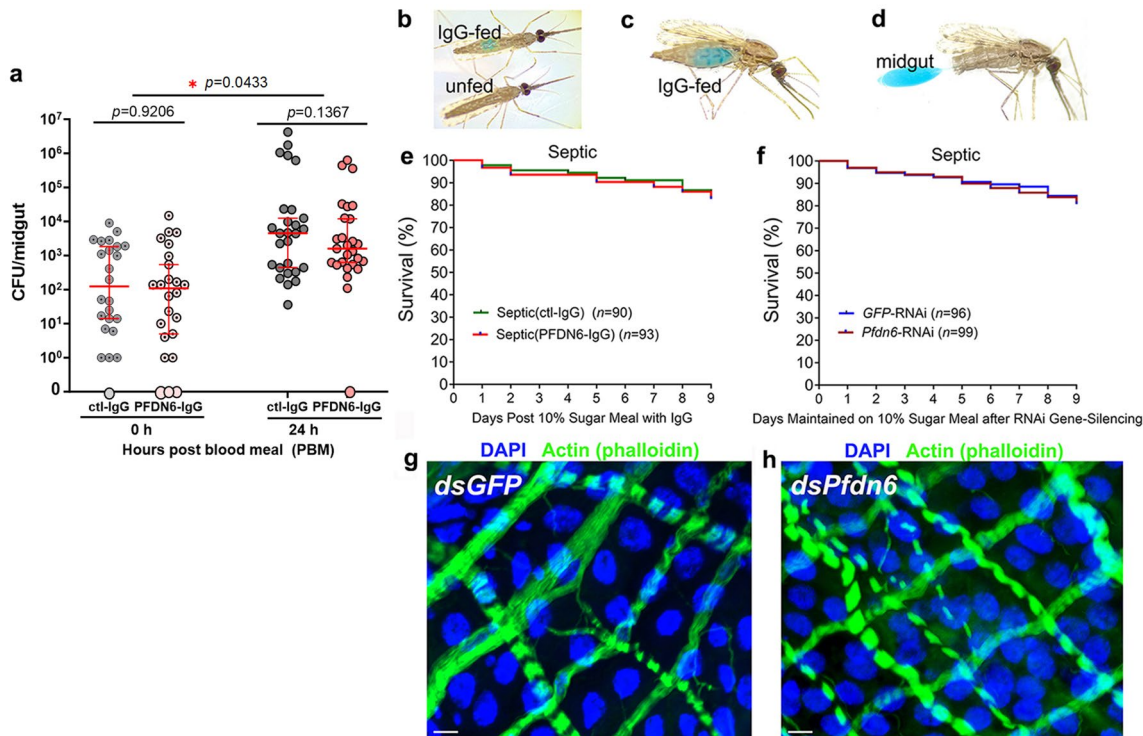
Extended Data Fig. 4 | The generation of a CRISPR/Cas9-mediated gene knockout of the *Pfdn6* gene resulted in pre-adult lethality of the larvae, indicating a somatic knockout mutant in the larval stage. Staining the gut's physical barriers and cell cytoskeleton with phalloidin (FITC) for filament (F)-actin revealed the degradation of the gut's physical barriers. **a**, Schematic representation of the plasmid construct generated to produce *Pfdn6*-gRNA (guide RNA) expressing transgenic mosquitoes and three gRNA target sequences were used to target one gene. **b**, Positive gRNA-expressing transgenic mosquitoes (named *Pfdn6*-gRNA) at larval and adult mosquitoes with red-fluorescence eyes were screened to generate homozygotes *Pfdn6*-gRNA-expressing transgenic mosquitoes. The X1 parental strain, which does not exhibit fluorescence in the eyes, was used as a control. **c**, Crossing *Pfdn6*-gRNA virgin female (red)

with *Vasa*::*Cas9* male (green, or named Cas9, or *Vasa*-*Cas9*) to generate transheterozygotes that were confirmed as somatic *Pfdn6* knockout (*Pfdn6*-KO) mutants through PCR and sequencing. Scale bars, 1 mm. **d**, Crossing of virgin female *Pfdn6*-gRNA with male Cas9 mosquitoes produced completely lethal (non-hatchable) eggs. **e**, Somatic knockout mutants (Transheterozygotes, *Pfdn6*/Cas9 KO) developed much slower at the larval stage (in orange circles) compared to the control *Vasa*::*Cas9* larvae (in green circles). **f**, **g**, The *Pfdn6*-KO (*Pfdn6*/Cas9 KO) died at the L3 or L4 larval stage (**f**), and Alexa-488-Phalloidin staining showed the degradation of the actin cytoskeleton (green) in the knockout mutants (*Pfdn6*-KO) compared to the control (*Vasa*::*Cas9*). DAPI: nuclei (blue). One representative image from at least 10 samples is shown. Z-stacks of 6 sections (each 0.1 μm thick) were captured using Zeiss LSM700. Scale bars, 10 μm.



Extended Data Fig. 5 | Co-immunoprecipitation (CoIP) analysis of PFDN6 with the total *A. gambiae* mosquitoes homogenate revealed interactions with actins 1–5, structural and extracellular matrix proteins, and immune factors. **a**, An illustration of the CoIP assay procedures. A total of 150 mosquitoes were injected with either PFDN6 recombinant protein (2.5 µg/µL in PBS) or with PBS alone as a negative control. Mosquitoes were left for 3 h after injection, and the mosquito tissues (guts, abdomen, thorax) were homogenized in an IP buffer (Tris 50 mM pH 7.9, NaCl 100 mM, EDTA 2 mM, BSA 0.1 µg/ml, Tween 20 0.1%, and protease inhibitors (Complete Mini, Roche)). After preclearance for 1 h, the supernatant was next incubated for 1 h with 1 µL PFDN6 antibody and subsequently with 30 µL of Protein A-Sepharose slurry (GE Healthcare) for another hour. Samples were centrifuged, and post-IP supernatant was collected. Sepharose beads were washed several times with alternating buffers: Tris-HCl (50 mM pH 7.9) with Tween 20 0.1% and Tris-HCl 50 mM pH 7.9 Tween 20 0.1% NaCl 500 mM buffers. **b**, Proteins eluted from the beads were run on Tris-Glycine

4–20% gradient SDS-PAGE gel followed by Colloidal Blue staining (Thermo Fisher Scientific). SeeBlue Plus (Thermo Fisher Scientific) was used as a protein ladder. Unique protein bands (AgPFD-40K, -80K, -140K) that differed from those in the PBS-injected control were excised and subjected to MASS-spec sequencing. Three biological replicates are included with the pooled samples from replicates that were subjected to Mass-spec sequencing. **c**, A summary of the functional groups of proteins identified interacting with the prefoldin complex, particularly with PFDN6 recombinant protein, is provided. Identified interacting proteins include cytoskeletal components such as Actin and Tubulin, basal lamina protein Laminin, extracellular matrix (ECM) proteins like Enolase, and immune factors such as Tep1, Tep15, and leucine-rich-repeat-containing protein LRIM26. Tep1 and Laminin were selected for further investigation to elucidate the role of PFDN6 as a host factor for *Plasmodium* parasites in the mosquito midgut. A detailed gene list and functional groups were included in Supplementary Table 3. Uncropped SDS-PAGE gel is in Supplementary Fig. 1.

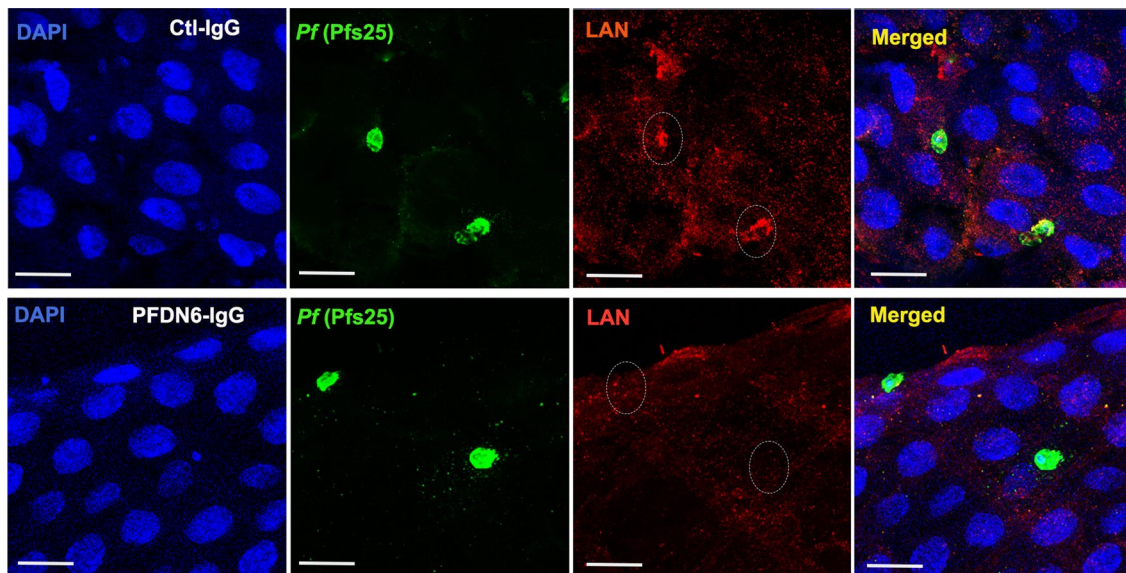


Extended Data Fig. 6 | The CFU (colony forming unit) assay measuring culturable bacteria in the mosquito midgut 24 h post blood meal (PBM) and RNAi-mediated gene silencing of *Pfdn6* or anti-PFDN6 co-feeding in the sugar meal does not compromise the integrity of the midgut physical barrier.

a, Bacteria proliferate in both control mosquitoes fed with control IgG (ctl-IgG) and the ones fed with anti-PFDN6 antibody (PFDN6-IgG). No significant difference in total bacterial loads in the gut lumen was observed in the leaky gut (PFDN6-IgG) compared to the controls (ctl-IgG). The total culturable bacterial number in the female mosquito midguts of control (ctl-IgG) or PFDN6-IgG mediated leaky gut at 0 h and 24 h PBM is reported (median±95% CI). At least three biological replicates with 9 midgut samples in each replicate are included ($n = 27$), each dot representing the number of bacteria in an individual midgut. Student's *t*-test (two-tailed) and one-way ANOVA were employed to calculate *p*-values and determine significance. **b-d**, Anti-PFDN6 were administered

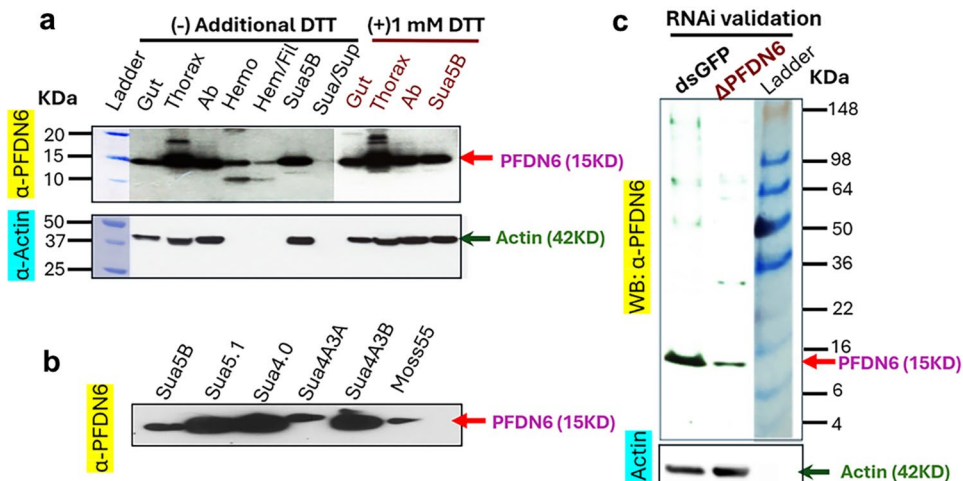
through the 10% sugar solution in a concentration of 400 μ g/mL with blue food dye added to confirm the delivery of PFDN6-IgG directly into the midguts.

e,f, Survival curves for mosquitoes co-fed with control antibody (ctl-IgG) or anti-PFDN6 antibody (PFDN6-IgG) with a 10% sugar meal (**d**) or subjected to RNAi-mediated gene silencing (3 d post-dsRNA injection) and maintained on a regular 10% sugar meal (**e**) under septic conditions. Kaplan-Meier survival analysis revealed no significant differences between groups, with three biological replicates included for each group. **g,h**, Confocal microscopy using Alexa-488-phalloidin staining to visualize the actin cytoskeleton (green) and DAPI staining to visualize nuclei (blue). The physical barrier of the midgut epithelium is well-integrated in both control (*dsGFP*) (**g**) and *Pfdn6* gene-silenced (*dsPfdn6*) (**h**) midguts. One representative image from at least ten midgut samples is shown. Z-stacks of 15 sections (each 0.1 μ m thick) were captured using Zeiss LSM700, and the final images were obtained by collapsing all Z-stacks. Scale bars, 10 μ m.



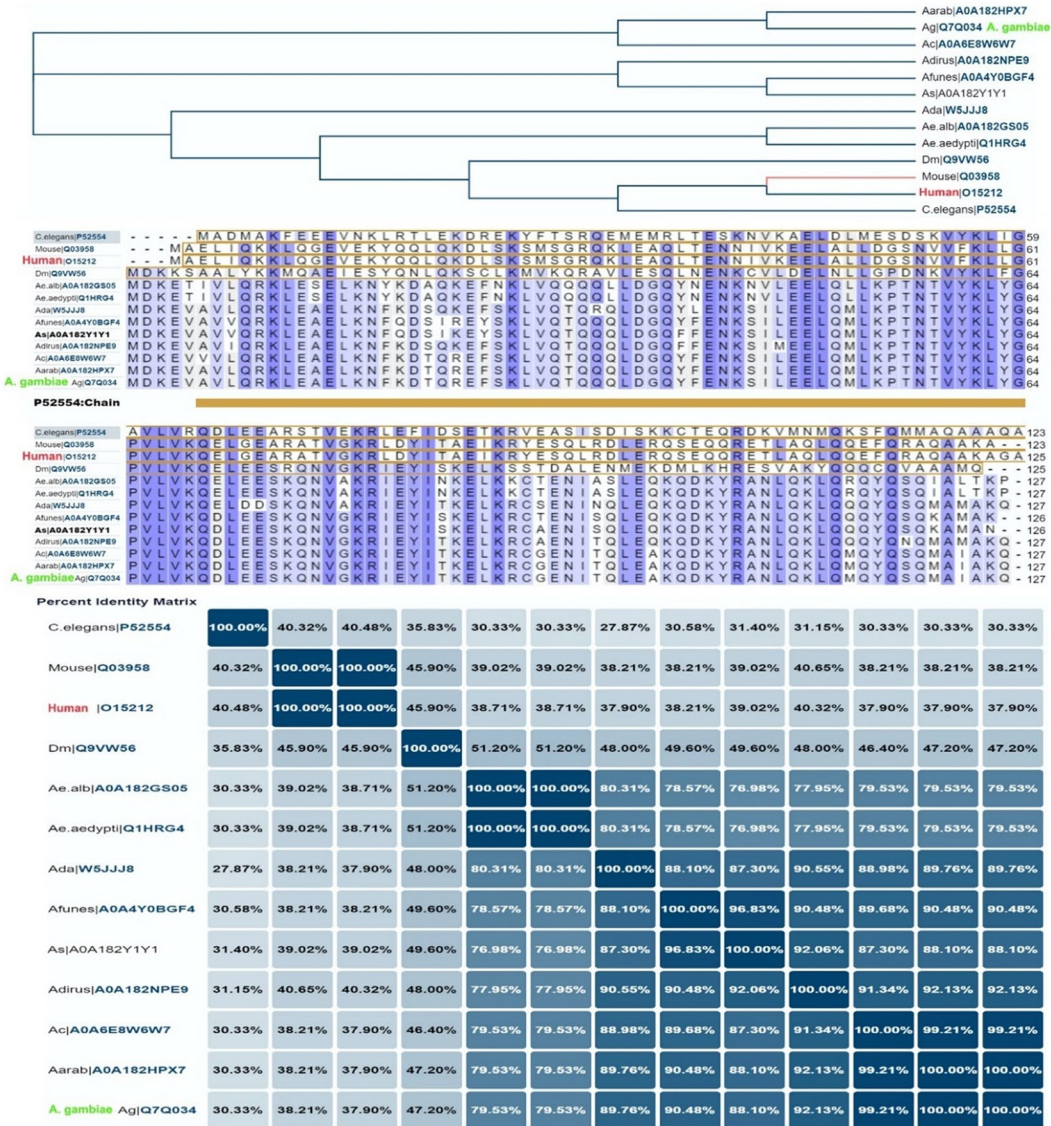
Extended Data Fig. 7 | Confocal microscopy analysis of co-blood-fed mosquito midguts using anti-PFDN6 antibody and *P. falciparum* gametocytes reveals the disruption of the prefoldin complex, leading to a leaky gut that allows Tep1 to co-localize more prominently on *P. falciparum* ookinetes within the leaky gut. The upper panel presents confocal images from mosquito midguts at 36 h post *P. falciparum* infectious blood meal, co-fed with control antibodies (Ctl-IgG), compared to mosquitoes fed on *P. falciparum*-infected blood meal introduced with PFDN6 antibodies (PFDN6-IgG). DAPI stains nuclei in blue, anti-

Pfs25 antibody stains *P. falciparum* ookinetes or early oocysts with Alexa-488 in green, and LAN indicates anti-Laminin antibody staining with Alexa-568 in red, illustrating the robust protection of laminin for the parasites in the presence of Laminin (LAN). Eclipse circles highlight areas where, in control mosquitoes, there is strong colocalization of Laminin masking the attack from parasites, whereas in the leaky gut, with barely noticeable staining of Laminin covers the parasites. One representative image is shown from at least ten midgut samples assayed with at least three ookinetes or oocysts in each gut. Scale bars, 10 μ m.



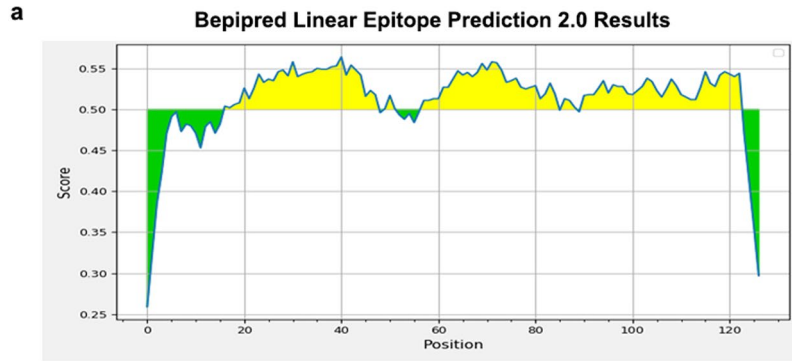
Extended Data Fig. 8 | Western blot analysis was conducted to profile the abundance of PFDN6 protein in different *A. gambiae* mosquito tissues and different *A. gambiae* cell lines and validation of *Pfdn6* RNAi gene silencing efficiency at protein level. **a**, PFDN6 protein was detected in the midgut (Gut), thorax, abdomen (Ab), whole perfused hemolymph with hemocytes (Hemo), filtered hemolymph (Hemo/Fil), mosquito Sua5B cell lysate (Sua5B), and filtered Sua5B cell supernatant (Sua/Sup). The presence of PFDN6 in the hemolymph but not in the Sua5B supernatant suggests its release into the hemolymph during cell damage and repair. The absence of PFDN6 in the filtered Sua5B cell culture supernatant indicates a positive correlation with cell damage in the mosquito guts. Protein levels were normalized using the Bradford assay, with 10 µg of total protein per sample. Anti-β-actin antibody (primarily bound to the nonfilamentous form of actin) served as the loading control, with actin absent in the hemolymph and Sua5B supernatant. For each replicate, 10 mosquitoes were

used for thorax or abdomen, 15 for midguts, and 50 for hemolymph. Samples were homogenized in RIPA buffer, subjected to SDS-PAGE (4–20% gradient Tris-Glycine gel), and treated with DTT at a final concentration of 1 mM. Primary antibodies used were PF DN6-IgG (1:1000) and anti-Actin (1:5000), with HRP as the secondary antibody (1:15,000). **b**, PF DN6 is presented in different *A. gambiae* cell lysates, using 10 µg of total protein as a load control. **c**, *Pfdn6*-RNAi gene silencing (Δ PFDN6) resulted in a significant decrease in the abundance of PF DN6 protein compared to control (*dsGFP*-injected mosquitoes), with Actin serving as the protein loading reference. The Fiji ImageJ quantification of Western blot densitometry revealed that PF DN6 protein was 87.8% less abundant in *Pfdn6*-gene-silenced mosquitoes compared to control mosquitoes (*dsGFP*-injected) using Actin as a normalization factor. Three replicates were performed, and one representative replicate is shown here. Uncropped immunoblots are shown in Supplementary Fig. 1.



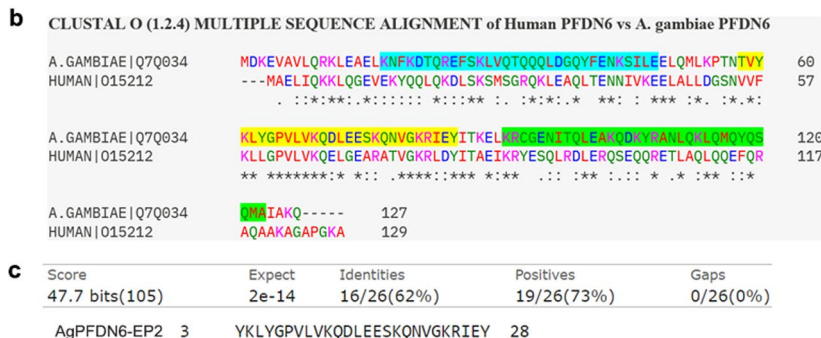
Extended Data Fig. 9 | Protein sequence alignment and phylogenetic analysis of PFDN6 in various organisms. A comprehensive protein sequence alignment was performed between mosquito prefoldin and its counterparts in humans, mice, *C. elegans*, and *Drosophila*, taking into account the potential cross-activity of prefoldin antibodies in mosquitoes, which might react off-target with human prefoldin when mosquito prefoldin is used as the transmission-blocking target. The alignment highlights a high degree of conservation in the PFDN6 protein at

the protein level within mosquito species, including *Anopheles* and *Aedes*, while showing significant divergence from human and mouse PFDN6 proteins from the Percent Identity Matrix analysis. Sequences were retrieved from UniProt and aligned using the Uniprot web service, employing Clustal Omega for multiple sequence alignment. The resulting phylogenetic tree, depicted as a cladogram, illustrates the evolutionary relationships among the prefoldin proteins across different species.



Predicted peptides:

No.	Start	End	Peptide	Length
1	17	48	KNFKDTQREFSKLVQTQQQLDGQYFENKSILE	32
2	58	85	TVYKLYGPVLVKQDLEESKQNVGKRIEY	28
3	91	123	KRCGENITQLEAKQDKYRANLQKLQMQYQSQMA	33



c

Score	Expect	Identities	Positives	Gaps
47.7 bits(105)	2e-14	16/26(62%)	19/26(73%)	0/26(0%)
AgPFDN6-EP2	3	YKLYGPVLVKQDLEESKQNVGKRIEY	28	
HumanPFDN6-EP2	3	+KL GPVLVKQ+L E VGKR +Y	28	
		FKLLGPVLVKQELGEARATVGKRLDY		

Extended Data Fig. 10 | In silico prediction of antibody epitopes for *A. gambiae* PFDN6 (AgPFDN6) and a comparison of sequence homology with human PFDN6 to evaluate potential cross-reactivity of prefoldin antibodies. This analysis is crucial for ensuring specificity when developing transmission-blocking vaccines. **a**, Epitope prediction for AgPFDN6 was performed using the IEDB Analysis Resource (<http://tools.iedb.org/bcell/>) with BepiPred Linear Epitope Prediction 2.0, identifying three predicted peptide epitopes (in the table below). **b**, Clustal O multiple sequence alignment of human PFDN6 and *A. gambiae* PFDN6, with predicted epitope peptide sequences highlighted in cyan (Epitope 1), yellow (Epitope 2), and green (Epitope 3). “**” indicates the residues are completely conserved; “:” denotes a strong similarity; “.” indicates

weak similarity. **c**, NCBI BlastP protein sequence homology analysis of the three peptide sequences shows that Epitope 2 (highlighted in yellow in panel **b**) exhibits high homology with 62% identity and 73% similarity to human PFDN6 Epitope 2. Epitope 1 shows no significant similarity found, and Epitope 3 shows 10/33 (30%) and 13/33 (39%) for Identities and Positives, respectively. This suggests potential cross-reactivity with Epitope 2 should be avoided when designing peptide antibodies for transmission-blocking vaccines. Epitope 1 demonstrates no significant similarity between human and mosquito PFDN6, making it a candidate worthwhile exploring for transmission-blocking vaccine potential.

Reporting Summary

Nature Portfolio wishes to improve the reproducibility of the work that we publish. This form provides structure for consistency and transparency in reporting. For further information on Nature Portfolio policies, see our [Editorial Policies](#) and the [Editorial Policy Checklist](#).

Statistics

For all statistical analyses, confirm that the following items are present in the figure legend, table legend, main text, or Methods section.

n/a Confirmed

- The exact sample size (n) for each experimental group/condition, given as a discrete number and unit of measurement
- A statement on whether measurements were taken from distinct samples or whether the same sample was measured repeatedly
- The statistical test(s) used AND whether they are one- or two-sided
Only common tests should be described solely by name; describe more complex techniques in the Methods section.
- A description of all covariates tested
- A description of any assumptions or corrections, such as tests of normality and adjustment for multiple comparisons
- A full description of the statistical parameters including central tendency (e.g. means) or other basic estimates (e.g. regression coefficient) AND variation (e.g. standard deviation) or associated estimates of uncertainty (e.g. confidence intervals)
- For null hypothesis testing, the test statistic (e.g. F , t , r) with confidence intervals, effect sizes, degrees of freedom and P value noted
Give P values as exact values whenever suitable.
- For Bayesian analysis, information on the choice of priors and Markov chain Monte Carlo settings
- For hierarchical and complex designs, identification of the appropriate level for tests and full reporting of outcomes
- Estimates of effect sizes (e.g. Cohen's d , Pearson's r), indicating how they were calculated

Our web collection on [statistics for biologists](#) contains articles on many of the points above.

Software and code

Policy information about [availability of computer code](#)

Data collection Data was collected in GraphPad Prism Version 10

Data analysis Data was analyzed in GraphPad Prism Version 10

For manuscripts utilizing custom algorithms or software that are central to the research but not yet described in published literature, software must be made available to editors and reviewers. We strongly encourage code deposition in a community repository (e.g. GitHub). See the Nature Portfolio [guidelines for submitting code & software](#) for further information.

Data

Policy information about [availability of data](#)

All manuscripts must include a [data availability statement](#). This statement should provide the following information, where applicable:

- Accession codes, unique identifiers, or web links for publicly available datasets
- A description of any restrictions on data availability
- For clinical datasets or third party data, please ensure that the statement adheres to our [policy](#)

The authors declare all data generated or analyzed in this study are included in the main body of the manuscript and figures, the Extended data figures, and Supplementary Information (Figures, Tables, Files). Source data for generating the main figures and Extended Data Figures are provided in the Excel files, and gel images and Western immunoblots are included in Supplementary Fig. 1. Additional information is available for the authors upon request.

Research involving human participants, their data, or biological material

Policy information about studies with [human participants or human data](#). See also policy information about [sex, gender \(identity/presentation\), and sexual orientation](#) and [race, ethnicity and racism](#).

Reporting on sex and gender

This was not a clinical trial. The goal of this minimal risk study was to collect blood from Plasmodium vivax-infected persons and artificially membrane feed this blood to mosquitoes. The analyzed output related to Plasmodium infection outcomes in the mosquitoes. No research intervention was applied to the blood donors. The blood donors were non-severe malaria outpatients attending malaria clinics along the Thai-Myanmar border. Either male or female volunteers were accepted enrollment, pregnant females were excluded. Sex was self-reported as was pregnancy. No analyses on blood donor sex or gender were performed. No consent was obtained for sharing individual-level data.

Reporting on race, ethnicity, or other socially relevant groupings

All Plasmodium vivax blood donor were of Asian race. Informed consent was performed in Thai, Burmese or Karen. No race or ethnicity information was collected. No analyses based on race, ethnicity or other social groupings were performed.

Population characteristics

Age was self-reported to confirm that subjects met the Inclusion Criteria requirement. No analyses based on age or other population demographics were performed.

Recruitment

Plasmodium vivax outpatients were identified during routine screening at malaria clinics along the Thai-Myanmar border. Positive persons were contacted by the study team and had the study explained to them to determine if they were willing to donate blood. If they were willing to join the study then informed consent was completed.

Ethics oversight

Both the Walter Reed Army Institute of Research Institutional Review Board and the Ethical Review Committee for Research in Human Subjects Ministry of Public Health, Thailand have reviewed and approved the study protocol (WRAIR#1949B).

Note that full information on the approval of the study protocol must also be provided in the manuscript.

Field-specific reporting

Please select the one below that is the best fit for your research. If you are not sure, read the appropriate sections before making your selection.

Life sciences Behavioural & social sciences Ecological, evolutionary & environmental sciences

For a reference copy of the document with all sections, see nature.com/documents/nr-reporting-summary-flat.pdf

Life sciences study design

All studies must disclose on these points even when the disclosure is negative.

Sample size

Mosquito and parasite numbers were counted by eye or using a Leica microscope. No sample-size calculation was performed. Mosquito sample sizes were based on mosquito and reagent availability and previous publications that were cited in the article. The standard sample sizes were used and would enable robust statistical analyses.

Data exclusions

No data were excluded from the analyses.

Replication

All experiments were replicated at least three times.

Randomization

Mosquitoes were randomly assigned to control or intervention groups.

Blinding

Investigators were blinded to treatment condition during data collection and analysis of the in vivo experiments.

Reporting for specific materials, systems and methods

We require information from authors about some types of materials, experimental systems and methods used in many studies. Here, indicate whether each material, system or method listed is relevant to your study. If you are not sure if a list item applies to your research, read the appropriate section before selecting a response.

Materials & experimental systems

n/a	Involved in the study
<input type="checkbox"/>	<input checked="" type="checkbox"/> Antibodies
<input type="checkbox"/>	<input checked="" type="checkbox"/> Eukaryotic cell lines
<input checked="" type="checkbox"/>	<input type="checkbox"/> Palaeontology and archaeology
<input type="checkbox"/>	<input checked="" type="checkbox"/> Animals and other organisms
<input checked="" type="checkbox"/>	<input type="checkbox"/> Clinical data
<input checked="" type="checkbox"/>	<input type="checkbox"/> Dual use research of concern
<input checked="" type="checkbox"/>	<input type="checkbox"/> Plants

Methods

n/a	Involved in the study
	<input checked="" type="checkbox"/> <input type="checkbox"/> ChIP-seq
	<input checked="" type="checkbox"/> <input type="checkbox"/> Flow cytometry
	<input checked="" type="checkbox"/> <input type="checkbox"/> MRI-based neuroimaging

Antibodies

Antibodies used

Tep1 polyclonal antibody: Boster Bio, cat# A02017-0.1 mg
 Laminin polyclonal antibody: Thermo Fisher Scientific, Cat# PA5-115490
 β-actin monoclonal antibody: Abcam, Cat# mAbcam 82260
 Pfs25 antibody: BEI resources, Cat# MRA-28
 Goat Anti-Rabbit IgG H&L (HRP): Abcam, Cat# ab6721
 Goat Anti-Mouse IgG H&L (HRP): Abcam, Cat# ab502719
 Goat anti-Rabbit IgG (H+L) Cross-Adsorbed Secondary Antibody, Alexa Fluor™ 488: Thermo Fisher Scientific, Cat# A-11008
 Goat anti-Mouse IgG (H+L) Cross-Adsorbed Secondary Antibody, Alexa Fluor™ 488: Thermo Fisher Scientific, Cat# A-11001
 Goat anti-Rabbit IgG (H+L) Cross-Adsorbed Secondary Antibody, Alexa Fluor™ 568: Thermo Fisher Scientific, Cat# A-11011
 Goat anti-Mouse IgG (H+L) Cross-Adsorbed Secondary Antibody, Alexa Fluor™ 568: Thermo Fisher Scientific, Cat# A-11004
 PFDN6 antibody: Washington Biotechnology generated polyclonal antiserum against recombinant PFDN6 protein in rabbit.
 GFP antibody: Washington Biotechnology generated polyclonal antiserum against recombinant GFP protein in rabbit.

Validation

The validation of all commercial primary antibodies for the species and application can be found on the manufacturer's websites, relevant citations, and antibody profiles in the online databases. The validation of the antibodies generated in this study is provided in the manuscript.

Eukaryotic cell lines

Policy information about [cell lines and Sex and Gender in Research](#)

Cell line source(s)

Sf9 cell: Sf9 cells in SF-900™ II SFM (Gibco, Thermo Fisher Scientific, Cat# 11496015)
 Sua5B cell: *A. gambiae* immune-competent cells, maintained in my lab.

Authentication

Describe the authentication procedures for each cell line used OR declare that none of the cell lines used were authenticated.

Mycoplasma contamination

Confirm that all cell lines tested negative for mycoplasma contamination OR describe the results of the testing for mycoplasma contamination OR declare that the cell lines were not tested for mycoplasma contamination.

Commonly misidentified lines (See [ICLAC](#) register)

Name any commonly misidentified cell lines used in the study and provide a rationale for their use.

Animals and other research organisms

Policy information about [studies involving animals; ARRIVE guidelines](#) recommended for reporting animal research, and [Sex and Gender in Research](#)

Laboratory animals

Anopheles gambiae mosquitoes: Keele strain, *A. stephensi* mosquitoes: Liston strain, *A. dirus* mosquitoes: AFRIMS strain.
 Swiss Webster mice: 8-week-old female

Wild animals

no wild animals were used in this study.

Reporting on sex

No field collected samples were used in this study.

Field-collected samples

Study did not involve samples collected from the field.

Ethics oversight

The protocol was approved by the Animal Care and Use Committee of Johns Hopkins University (permit number MO15H144 for regular blood feeding and *P. berghei* infection, MO128H76 for mice immunization with recombinant proteins).
 For *Plasmodium vivax* study: Both the Walter Reed Army Institute of Research Institutional Review Board and the Ethical Review Committee for Research in Human Subjects Ministry of Public Health, Thailand, have reviewed and approved the study protocol (WRAIR#1949B).

Note that full information on the approval of the study protocol must also be provided in the manuscript.

Plants

Seed stocks

Report on the source of all seed stocks or other plant material used. If applicable, state the seed stock centre and catalogue number. If plant specimens were collected from the field, describe the collection location, date and sampling procedures.

Novel plant genotypes

Describe the methods by which all novel plant genotypes were produced. This includes those generated by transgenic approaches, gene editing, chemical/radiation-based mutagenesis and hybridization. For transgenic lines, describe the transformation method, the number of independent lines analyzed and the generation upon which experiments were performed. For gene-edited lines, describe the editor used, the endogenous sequence targeted for editing, the targeting guide RNA sequence (if applicable) and how the editor was applied.

Authentication

Describe any authentication procedures for each seed stock used or novel genotype generated. Describe any experiments used to assess the effect of a mutation and, where applicable, how potential secondary effects (e.g. second site T-DNA insertions, mosaicism, off-target gene editing) were examined.

Terms and Conditions

Springer Nature journal content, brought to you courtesy of Springer Nature Customer Service Center GmbH (“Springer Nature”).

Springer Nature supports a reasonable amount of sharing of research papers by authors, subscribers and authorised users (“Users”), for small-scale personal, non-commercial use provided that all copyright, trade and service marks and other proprietary notices are maintained. By accessing, sharing, receiving or otherwise using the Springer Nature journal content you agree to these terms of use (“Terms”). For these purposes, Springer Nature considers academic use (by researchers and students) to be non-commercial.

These Terms are supplementary and will apply in addition to any applicable website terms and conditions, a relevant site licence or a personal subscription. These Terms will prevail over any conflict or ambiguity with regards to the relevant terms, a site licence or a personal subscription (to the extent of the conflict or ambiguity only). For Creative Commons-licensed articles, the terms of the Creative Commons license used will apply.

We collect and use personal data to provide access to the Springer Nature journal content. We may also use these personal data internally within ResearchGate and Springer Nature and as agreed share it, in an anonymised way, for purposes of tracking, analysis and reporting. We will not otherwise disclose your personal data outside the ResearchGate or the Springer Nature group of companies unless we have your permission as detailed in the Privacy Policy.

While Users may use the Springer Nature journal content for small scale, personal non-commercial use, it is important to note that Users may not:

1. use such content for the purpose of providing other users with access on a regular or large scale basis or as a means to circumvent access control;
2. use such content where to do so would be considered a criminal or statutory offence in any jurisdiction, or gives rise to civil liability, or is otherwise unlawful;
3. falsely or misleadingly imply or suggest endorsement, approval , sponsorship, or association unless explicitly agreed to by Springer Nature in writing;
4. use bots or other automated methods to access the content or redirect messages
5. override any security feature or exclusionary protocol; or
6. share the content in order to create substitute for Springer Nature products or services or a systematic database of Springer Nature journal content.

In line with the restriction against commercial use, Springer Nature does not permit the creation of a product or service that creates revenue, royalties, rent or income from our content or its inclusion as part of a paid for service or for other commercial gain. Springer Nature journal content cannot be used for inter-library loans and librarians may not upload Springer Nature journal content on a large scale into their, or any other, institutional repository.

These terms of use are reviewed regularly and may be amended at any time. Springer Nature is not obligated to publish any information or content on this website and may remove it or features or functionality at our sole discretion, at any time with or without notice. Springer Nature may revoke this licence to you at any time and remove access to any copies of the Springer Nature journal content which have been saved.

To the fullest extent permitted by law, Springer Nature makes no warranties, representations or guarantees to Users, either express or implied with respect to the Springer nature journal content and all parties disclaim and waive any implied warranties or warranties imposed by law, including merchantability or fitness for any particular purpose.

Please note that these rights do not automatically extend to content, data or other material published by Springer Nature that may be licensed from third parties.

If you would like to use or distribute our Springer Nature journal content to a wider audience or on a regular basis or in any other manner not expressly permitted by these Terms, please contact Springer Nature at

onlineservice@springernature.com